IPP-Report

IPP Max-Planck-Institut für Plasmaphysik

Alexander Chih-Yao Teo

One-Dimensional Model of Global Alfvén Eigenmodes inTortus and Wendelstein VII-AS

Dissertation

IPP III/231

Juli 1998

One-Dimensional Model of Global Alfvén Eigenmodes in TORTUS and Wendelstein WVII-AS

Chih-Yao Teo
Max-Planck-Institut für Plasmaphysik,
IPP-EURATOM Association, Germany.

September 1997

In this article, a model for GAEs in a screw pinch plasma geometry is presented. The wave equations are derived from an ideal MHD model with corrections for finite frequency [1]. Analytical and numerical solutions of these equations, applied to parameter sets approximating the TORTUS Tokamak and the Wendelstein WVII-AS Advanced Stellarator, are presented and discussed.

1 Ideal MHD Equations with Finite Frequency Corrections

The MHD equations used in this model are:

$$\begin{aligned}
\rho \frac{\partial \vec{v}}{\partial t} &= \vec{J} \times \vec{B} && \text{FLUID EQUATION OF MOTION} \\
\vec{E} + \vec{v} \times \vec{B} &= \frac{1}{n_e q_e} \left(\vec{J} \times \vec{B} \right) && \text{OHM'S LAW} \\
\vec{\nabla} \times \vec{B} &= \mu_0 \vec{J} && \text{AMPERE'S LAW} \\
\vec{\nabla} \times \vec{E} &= -\frac{\partial \vec{B}}{\partial t} && \text{FARADAY'S LAW}
\end{aligned} \tag{1}$$

The plasma is assumed to be perfectly conducting, that is, to not have any ohmic resistivity. The plasma particles are also assumed to be "cold", that is, to have no thermal motion. There is hence no kinetic pressure. Ignoring the plasma pressure means that the Slow Wave will not appear in this model.

Also neglected in this model are electron parallel dynamics. This is equivalent to assuming that the electrons have no inertia, or in other words, that the electrons are massless, $m_e \to 0$. The effect of this term on the plasma model is discussed by Cross and Miljak [2]. Neglecting the electron mass means that the Surface Quasi-Electrostatic Wave will also not appear in this model. While this wave mode is still relevant to the frequency range which will be under consideration, the propagation of these localized surface waves does not affect the global nature of the GAEs and is therefore neglected.

Perturbations of the form in equation (1.2) are introduced to the model and the equations linearized. The following perturbation expansions are made:

$$\begin{array}{rcl} \vec{B} & = & \vec{B_0} + \vec{b} \\ \vec{J} & = & \vec{J_0} + \vec{j} \\ \vec{E} & = & \vec{e} \\ \vec{v} & = & \vec{v} \end{array} \tag{2}$$

where $\vec{b}$, $\vec{j}$, $\vec{e}$ and $\vec{v}$ are wave-associated perturbations.

It is assumed that there are no steady-state electric fields acting on the plasma ($\vec{E_0} = 0$) and that the plasma is static ($\vec{v_0} = 0$). The MHD formulation requires that we neglect density perturbations so as to remain consistent with the continuity equation

$$\frac{\partial n}{\partial t} + \vec{\nabla} . (n\vec{v}) = 0 \tag{3}$$

where n represents the particle density.

2 Plasma Equilibrium and Screw Pinch Geometry

The plasma in considered in the cylindrical approximation and is assumed to have a magnetic field configuration with a poloidal component $B_\theta(r)$ and an axial component $B_z(r)$ but no radial component $B_r(r) = 0$. Thus, the equilibrium magnetic field can be expressed as

$$\vec{B_0} = 0\vec{r} + B_\theta(r)\vec{\theta} + B_z(r)\vec{z} \tag{4}$$

where unit vectors in the three directions are given by $\vec{r}$, $\vec{\theta}$ and $\vec{z}$.

A perfectly conducting wall [3] surrounds the plasma at a radius of $r = a$. This gives us a set of boundary conditions to be satisfied at the plasma edge, which are

$$\begin{array}{rcl} \vec{\nabla} \times \vec{e}|_{r=a} & = & 0 \\ \vec{\nabla} . \vec{b}|_{r=a} & = & 0 \end{array} \tag{5}$$

where $\vec{e}$ and $\vec{b}$ are wave-associated electric and magnetic field perturbations.

Non-perturbation (*equilibrium*) quantities are assumed to be independent of the poloidal coordinate θ and the axial coordinate z; instead functions solely of the radial coordinate r. The length of the cylinder is $2\pi R$, where R is the major radius of the torus which this cylinder approximates, which means that the cylinder has the same length as the axis of a torus with a major radius of R. *Periodic boundary conditions* are assumed in the z-direction, that is, all quantities are assumed to be identical on the surfaces at $z = 0$ and $z = 2\pi R$.

All global perturbations are, on the other hand, periodic in both the poloidal and axial directions, so the perturbations in (2) can be expressed as

$$f(\vec{x}, t) = f(\vec{x}) \exp[i(-\omega t + \vec{k}.\vec{x})] = f(r) \exp\left[i(-\omega t + m\theta + \frac{n}{R}z)\right] \tag{6}$$

where the integers m and n are respectively the poloidal and toroidal mode numbers. The (m,n) wave mode has m nodes in the poloidal direction and n nodes in the toroidal (axial) direction.

In this expansion for all global perturbations, wave modes with positive poloidal mode numbers m propagate in the $+\vec{\theta}$ direction and those with negative m propagate in the $-\vec{\theta}$ direction. Similarly, perturbations with positive toroidal mode numbers n propagate in the $+\vec{z}$ direction and those with negative n propagate in the $-\vec{z}$ direction. The standard right-hand cylindrical coordinate axes have been adopted, where $\vec{r} \times \vec{\theta} = \vec{z}$.

The plasma is assumed to have electron density and current density profiles, respectively $n_e(r)$ and $\vec{J_0}(r)$, which also vary solely in the radial direction. These profiles are specified input parameters to the model. *Static Equilibrium* is also assumed, that is, that the plasma satisfies the conditions given by

$$\begin{aligned} \vec{J_0} \times \vec{B_0} &= 0 \qquad \text{FORCE BALANCE} \\ \vec{\nabla} \times \vec{B_0} &= \mu_0 \vec{J_0} \qquad \text{AMPERE'S LAW} \\ \vec{\nabla}.\vec{B_0} &= 0 \qquad \text{DIVERGENCE OF } \vec{B} \end{aligned} \tag{7}$$

which results in $B_\theta(r)$ and $B_z(r)$ profiles which are given by

$$\begin{aligned} B_\theta(r) &= \frac{\mu_0}{r} \int_0^r \vec{J_0}(r').\vec{z}\; r'\, dr' \\ B_z(r) &= B_z(0) - \mu_0 \int_0^r \vec{J_0}(r').\vec{\theta}\; dr' \end{aligned} \tag{8}$$

and the further condition that $\vec{J_0}(r).\vec{r} = 0$. $B_z(0)$ is an input parameter.

A further assumption is that the plasma contains just a single ion species and is electrically neutral, so the ion density profile is related to the electron density profile simply by

$$q_i n_i(r) = q_e n_e(r) \tag{9}$$

where q_i and q_e are the ion and electron charges.

The local safety factor is defined in cylindrical geometry as

$$q(r) = \frac{r\, B_z(r)}{R\, B_\theta(r)} \tag{10}$$

and the input of an equilibrium $q(r)$ profile is also possible, to allow for the use of equilibria calculated by another program, for instance, a Grad-Shafranov solver. Stellarator rotational transform profiles $\iota(r)$ can be input by using the relation $q(r) = 1/\iota(r)$.

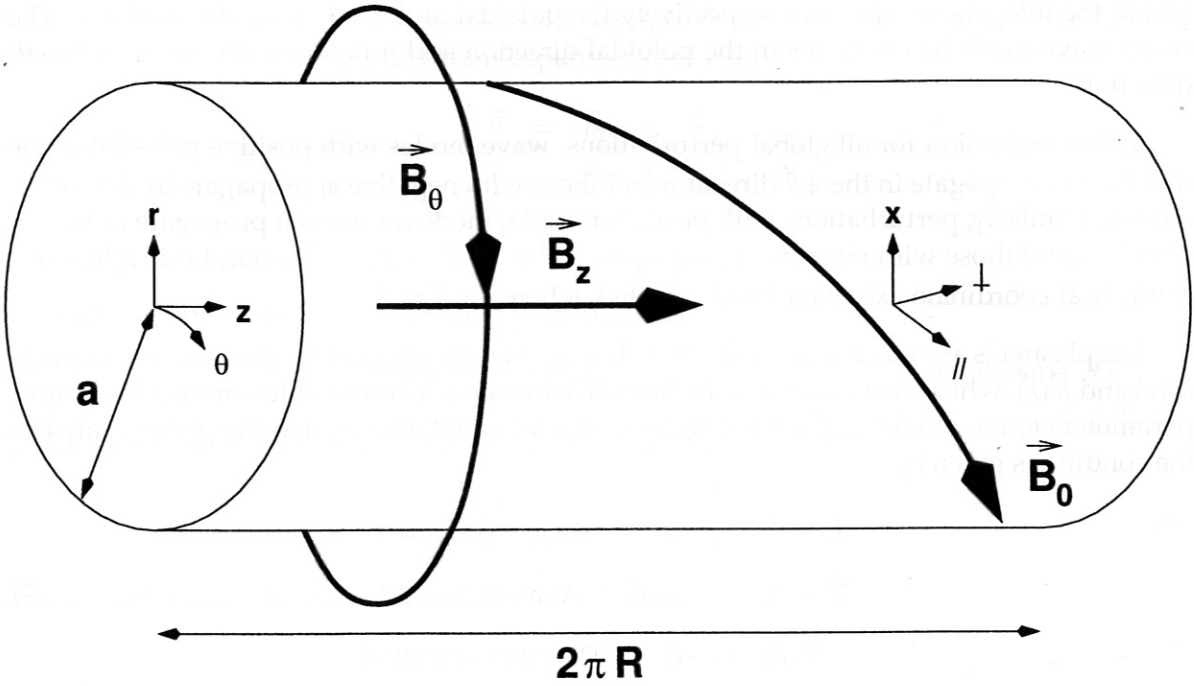

Figure 1: Screw Pinch geometry. The cylindrical $(\vec{r}, \vec{\theta}, \vec{z})$ coordinates are rotated to obtain a new system $(\vec{r}, \vec{\|}, \vec{\perp})$ where $\vec{\|}$ is aligned along the background magnetic field $\vec{B}_0$. The length of the plasma column is $2\pi R$, where R is the major radius of the toroidal plasma being modelled, and the radius of the column is a, the minor radius of the plasma.

Figure 1 shows a plasma model in *screw pinch* geometry. From our cylindrical system, the radial coordinate r is retained, but normalized to the minor radius a with a new radial coordinate $x = r/a$. A unit radial vector is denoted by $\vec{x}$. In addition, the coordinate axes are rotated so that one of them, $\|$, is now parallel to the local background magnetic field $\vec{B}_0$. A unit "parallel" vector is given by $\vec{\|} = \vec{B}_0/|\vec{B}_0|$. To keep the coordinate system orthogonal, a third coordinate, $\perp$, is chosen such that a unit "perpendicular" vector is given by $\vec{\perp} = \vec{\|} \times \vec{x}$.

In this geometry, the wave vector components are given by

$$\begin{aligned} \vec{k}\,.\,\vec{B}_0 &= k_\| B_0 = \frac{m}{r} B_\theta(r) + \frac{n}{R} B_z(r) \\ (\vec{k} \times \vec{B}_0)_r &= \frac{m_\perp}{r} B_0 = -\frac{n}{R} B_\theta(r) + \frac{m}{r} B_z(r) \end{aligned} \tag{11}$$

and the wave magnetic field components are given by

$$\begin{aligned} \vec{b}\,.\,\vec{B}_0 &= b_\| B_0 = b_\theta B_\theta(r) + b_z B_z(r) \\ (\vec{b} \times \vec{B}_0)_r &= b_\perp B_0 = -b_z B_\theta(r) + b_\theta B_z(r) \end{aligned} \tag{12}$$

3 Linearized Wave Dispersion Relations

The MHD equations (1) are cast in the screw-pinch coordinate system and all terms involving $\vec{J}_0$ and $\vec{j}$ are eliminated. For cleanliness, the quantities $p_\| = i\omega b_\|$ and $\mathcal{E}_\perp = e_\perp/a$ are intro-

duced. After some algebraic manipulation of the linearized equations, Ballico and Cross [4] obtain a set of two coupled first-order partial differential equations

$$\begin{aligned} \frac{\partial p_{\parallel}}{\partial x} &= -\ T_1 p_{\parallel} \ -\ T_2 \mathcal{E}_{\perp} \\ \frac{\partial \mathcal{E}_{\perp}}{\partial x} &= \quad\ T_3 p_{\parallel} \ +\ T_4 \mathcal{E}_{\perp} \end{aligned} \tag{13}$$

where

$$\begin{aligned} T_1 &= \frac{1}{x}\left[\frac{m_{\perp}}{F_0}(G_0 + K_{\parallel} S_0) \ +\ \frac{B_{\theta}^2}{B_0^2}\right] \\ T_2 &= K_{\Lambda}^2 \ +\ H_0 \\ T_3 &= 1 \ -\ \frac{m_{\perp}^2}{x^2 F_0} \\ T_4 &= \frac{1}{x}\left[\frac{m_{\perp}}{F_0}(G_0 + K_{\parallel} S_0) \ -\ \frac{B_z^2}{B_0^2}\right] \end{aligned} \tag{14}$$

and

$$\begin{aligned} K_{\Lambda}^2 &= \frac{F_0^2 - G_0^2}{F_0} \\ K_{\parallel} &= \frac{1}{B}\left(\frac{m}{x} B_{\theta} \ +\ \frac{na}{R} B_z\right) \\ F_0 &= A_0 \ -\ K_{\parallel}^2 \\ G_0 &= \Omega A_0 \ - D_0 K_{\parallel} \\ S_0 &= D_0 \ -\ 2\frac{B_{\theta} B_z}{x} \\ H_0 &= \frac{S_0}{F_0}(F_0 D_0 - A_0 S_0 - 2 G_0 K_{\parallel}) \\ A_0 &= \frac{\Omega^2 N}{1 - \Omega^2} \\ D_0 &= \frac{1}{B^2}\left(B_z \frac{\partial B_{\theta}}{\partial x} \ -\ B_{\theta} \frac{\partial B_z}{\partial x} + \frac{B_{\theta} B_z}{x}\right) \\ N &= \frac{\mu_0 q_i^2 a^2 n_i}{m_i} \\ \Omega &= \frac{\omega}{\omega_{ci}} \\ \omega_{ci} &= \frac{q_i B_0}{m_i} \end{aligned} \tag{15}$$

The eigenvector of the solution $(p_{\parallel}, \mathcal{E}_{\perp})$ in the equations (13) gives us the wave fields $b_{\parallel}$ and $e_{\perp}$. The other wave fields can be calculated from solving Ampere's Law and Faraday's Law (1). Transformation back into standard cylindrical (r, θ, z) geometry can be done using (12).

The term labelled K_{Λ} in (15) represents the wave vector in both directions non-parallel to

the background field. The equation

$$K_\Lambda^2 = (|\vec{k}|^2 - k_\parallel^2)a^2 = \frac{F_0^2 - G_0^2}{F_0} \tag{16}$$

is in fact the wave dispersion relation for MHD waves in this model.

3.1 The Alfvén Resonance

The wave dispersion relation (16) has a resonance when $F_0 = 0$. This resonance is the *Alfvén resonance*, and it occurs at the *Alfvén frequency*

$$\omega_A(x) = \frac{|k_\parallel(x)|v_A(x)}{\sqrt{1 + k_\parallel^2(x)v_A^2(x)/\omega_{ci}}} \approx |k_\parallel(x)|v_A(x) \tag{17}$$

where

$$v_A(x) = \frac{B_0(x)}{\sqrt{\mu_0 m_i n_i(x)}} \tag{18}$$

is the *Alfvén speed*.

The Alfvén resonance is mathematically a spatial non-square-integrable logarithmic singularity and in this simple model without damping, it manifests itself as the infinitely thin layer corresponding to the surface where the condition of resonance (17) is satisfied giving a perpendicular wave vector $k_\perp = \infty$. On this surface, an Alfvén wave with $k_\perp = \infty$ will have the same frequency ω and parallel wave vector $k_\parallel$ as the Fast Wave. The Fast Wave propagates with $k_\perp^2 > 0$ on the high-density side of this surface, and the Alfvén wave on the low density side, in a narrow layer where $k_\perp^2 \in (0, \infty)$.

In cylindrical configurations, the Alfvén resonance results in a wave solutions for each wave mode (m, n) over a continuous range of frequencies, the *Alfvén continuum spectra*. Assuming that $k_\parallel$ is constant for the time being, Alfvén resonance surface moves continuously within this range with increasing frequency ω, from the region of small v_A to the region of large v_A. This often, but not always, corresponds to moving from the centre of the plasma, where the mass density is high, to the edge, where the mass density is low. Now allowing $k_\parallel$ to vary, but with k_z still constant as it is determined entirely by the toroidal mode number n, we may get continua which have minima at different locations in the plasma due to the variation of $k_\parallel$ with the radial coordinate x. Continua may have minima at zero wave frequency $\omega = 0$.

In non-cylindrically-symmetric plasma configurations, breaks in the symmetry in the poloidal direction lead to coupling between the poloidal mode numbers m. Breaks in the symmetry in the toroidal direction lead, on the other hand, to coupling between the toroidal mode numbers n.

Approximate two-dimensional (tokamak) equilibria can be calculated using an asymptotic expansion [5] in terms of the inverse aspect ratio $\epsilon \stackrel{\text{def}}{=} a / R$, where a is the effective plasma minor radius and it is assumed that $\epsilon \ll 1$. The poloidal flux function is expanded

$$\psi(x, \theta) \stackrel{\text{def}}{=} \int \vec{B}_\theta . d\vec{A} = \psi_0(x) + \psi_1(x, \theta) + \psi_2(x, \theta) + \psi_3(x, \theta) + \ldots \tag{19}$$

where for each integer value ℓ, $\psi_\ell(x,\theta)/\psi_0(x) = \mathcal{O}(\epsilon^\ell)$. The term $\psi_0(x)$ corresponds to the cylindrical flux function.

Solving the ideal MHD equations in this flux system and retaining only the ψ_0 and ψ_1 terms gives us dispersion relations for the coupled Alfvén continua of the modes (m,n) and $(m+1,n)$, dispersion relations with "toroidal corrections". Fu and Van Dam [6] give the result of this calculation as

$$\omega^2_{A\pm}(x) \;=\; v^2_A(x)\,\frac{k^2_{\|m} + k^2_{\|m+1} \pm \sqrt{(k^2_{\|m} - k^2_{\|m+1})^2 + 9\epsilon^2 x^2 k^2_{\|m} k^2_{\|m+1}}}{2(1-\frac{9}{4}\epsilon^2 x^2)} \tag{20}$$

At the surface at a radial distance of x_0 from the magnetic axis, where the local safety factor $q(x_0) = (m+\frac{1}{2})/n$, the *cylindrical* Alfvén continua of the modes (m,n) and $(m+1,n)$ cross each other. On this surface, the parallel components of their wave vectors are related by $k_{\|m}(x_0) = -k_{\|m+1}(x_0)$ and coupling of the two continua results in an "avoided crossing", a gap of width $\delta\omega = \omega_{A+} - \omega_{A-} \approx 2\epsilon x_0 |k_{\|m}(x_0) v_A(x_0)|$.

Now, retaining only the ψ_0 and ψ_2 terms in equation (19), we obtain the dispersion relations for the coupled Alfvén continua of the modes (m,n) and $(m+2,n)$, dispersion relations with "elliptical corrections". Betti and Freidberg [7] give the result of this calculation as

$$\omega^2_{A\pm}(x) \;=\; v^2_A(x)\,\frac{k^2_{\|m} + k^2_{\|m+2} \pm \sqrt{(k^2_{\|m} - k^2_{\|m+2})^2 + 16H'^2 k^2_{\|m} k^2_{\|m+2}}}{2(1-4H'^2)} \tag{21}$$

where $H' = \partial H/\partial x$, the *elliptical distortion* H satisfies the equation

$$\frac{d}{dx}\left(xB^2_\theta \frac{dH}{dx}\right) - 3\frac{B^2_\theta}{x} H \;=\; 0 \tag{22}$$

$$H(0) = 0 \qquad H(1) = -a(\kappa-1)/2$$

and the plasma elongation $\kappa \stackrel{\text{def}}{=} (\text{cross-sectional area})/\pi a^2$.

At the surface at a radial distance of x_0 from the magnetic axis, where the local safety factor $q(x_0) = (m+1)/n$, the *cylindrical* Alfvén continua of the modes (m,n) and $(m+2,n)$ cross each other. On this surface, the parallel components of their wave vectors are related by $k_{\|m}(x_0) = -k_{\|m+2}(x_0)$ and coupling of the two continua results in an "avoided crossing", a gap of width $\delta\omega = \omega_{A+} - \omega_{A-} \approx 2H'(x_0) v_A(x_0)/q(x_0)R$.

In general, retention of the term ψ_ℓ along with the cylindrical term ψ_0 and solution of the MHD equations with these two terms in the expansion (19) results in a system where the modes (m,n) and $(m+\ell,n)$ are coupled. If a surface satisfying $q(x_0) = (m+\frac{\ell}{2})/n$ exists within the plasma (for some $x \in [0,1]$), the cylindrical continua will cross at the radial position $x = x_0$, where the common Alfvén frequency of the two modes is given by

$$\omega_{A0} \;=\; \frac{v_A(x_0)\ell}{2q(x_0)R} \tag{23}$$

If $\psi_\ell \neq 0$, coupling of the two continua leads to a gap, whose width $\delta\omega$ is determined by the relative magnitude of the non-cylindrical term ψ_ℓ/ψ_0.

3.2 Discrete Eigenmode Solutions: GAEs

In a homogeneous plasma, elimination of the $\mathcal{E}_\perp$ terms from the system of differential equations (13) using Faraday's Law (1) renders a single second-order partial differential equation

$$\frac{\partial^2 p_\parallel}{\partial x^2} + \frac{1}{x}\frac{\partial p_\parallel}{\partial x} + \left(K_\Lambda^2 - \frac{m_\perp^2}{x^2}\right) p_\parallel = 0 \tag{24}$$

which is consistent with the relation $\vec{\nabla}.\vec{b} = 0$.

We place a condition on our equilibria, that $m_\perp$ varies very slowly with x at the axis of symmetry, that is, that the plasma is approximately homogeneous near $x = 0$. Equation (24) is then the Bessel differential equation, which has the solution

$$p_\parallel = p_0 J_m(K_\Lambda x) \qquad \text{when } K_\Lambda^2 > 0 \tag{25}$$

where p_0 is an arbitrary amplitude factor, J_m is the Bessel function of degree m and at the axis of symmetry $x = 0$, $m_\perp = m$, the poloidal wave number (from equation 11).

We thus now have a condition for $p_\parallel$ at $x = 0$. From equation (5), we have a second boundary condition, that for $\mathcal{E}_\perp$ at the wall $x = 1$, namely, $\mathcal{E}_\perp(x)|_{x=1} = 0$. Thus we now desire the solution to a set of two coupled differential equations (13), satisfying one boundary condition at $x = 0$ and another boundary condition at $x = 1$. This belongs to a class of mathematical problems known as *two point boundary value problems* [8].

For a wave mode (m, n), there is a continuous spectrum of wave solutions, corresponding to the Alfvén continuum of the wave mode, for frequencies within this continuum. If this continuum does not extend to wave frequency $\omega = 0$, there usually exists a series of discrete eigensolutions to the partial differential equations (13) at frequencies just below the lower end of the Alfvén continuum. These eigensolutions, upon examination of their eigenvectors, are cavity oscillations of the entire system subject to its boundary conditions, global eigenmodes of the Alfvén wave. These are the *Global Alfvén Eigenmodes* (GAEs).

In cylindrical geometry, Alfvén continua of modes sharing toroidal mode numbers n do not couple to each other. Differential equations featuring two-dimensional "correction" terms based on the asymptotic expansion (19) have not been included, so this model is not able to find the "gap modes" such as the Toroidal Alfvén Eigenmodes (TAEs) and Elliptical Alfvén Eigenmodes (EAEs). Equation (23) can, however, be used to obtain a reasonable approximation for their frequencies.

Absence of kinetic pressure means that the Beta-induced Alfvén Eigenmodes (BAEs) also do not feature in the spectrum of eigensolutions of this model.

The structure of the Alfvén continua of various wave modes in the screw pinch geometry can be determined in this model using equation (17). Possible coupling between different continuum layers is also investigated using equations (20) and (21). A search is then carried out for GAEs at frequencies just below the minimum Alfvén frequency in the plasma. This is done by seeking a solution to the two point boundary value problem in this frequency range, using a shooting method involving a standard Fourth Order Stepsize-Controlled Runge-Kutta numerical integrator and a Brent's Method root finder.

Major radius	R	=	0.44 m
Minor radius	a	$\leq$	0.11 m
Toroidal magnetic field	B_ϕ	$\leq$	1.3 T
Toroidal plasma current	I_p	$\leq$	40 kA
Ion temperature	T_i	$\leq$	100 eV
Electron temperature	T_e	$\leq$	300 eV
Electron density	n_e	$\leq$	4×10^{19} m^{-3}
Pulse length	τ	$\leq$	40 ms

Table 1: Vessel and plasma parameters of TORTUS.

4 TORTUS High-Current Plasmas

The TORTUS Tokamak is a small plasma fusion research device, designed and built in the Plasma Physics Department, University of Sydney, New South Wales, Australia. Table 1 shows a summary of the vessel and plasma parameters of TORTUS. The maximum values have not been observed simultaneously.

4.1 Input Parameters

In this one-dimensional model, the TORTUS plasma is assumed to have a major radius of $R = 0.44$ m, giving a length of the screw pinch plasma of $2\pi R = 2.76$ m, and a minor radius of $a = 0.10$ m. Perfectly conducting walls surround the plasma at the radial position $r = a$, where the boundary conditions (5) are applied. These values of R and a give an inverse aspect ratio parameter of $\epsilon = 0.227$ in the asymptotic expansion (19) for approximate two-dimensional equilibria. The TORTUS plasma is assumed to have a circular cross-section, thus all the expansion terms $\psi_\ell = 0$ for $\ell \geq 2$ in (19).

A fully-ionized hydrogen plasma is modelled here, with a total plasma current of $I_p = -36.5$ kA, an on-axis equilibrium magnetic field of $B_z(0) = 1.2$ T and an on-axis electron density of $n_e(0) = 2.4 \times 10^{19}$ m^{-3}. The negative sign on I_p indicates that the magnetic field and the plasma current are in the opposite directions.

The plasma current is assumed to have a parabolic-squared density profile, satisfying $J_0(x) = J_0(0)[1 - 2x^2 + x^4]$. Integration over the entire cross-section, where $I_p \stackrel{\text{def}}{=} \int_0^{2\pi} d\theta \int_0^1 x\, dx\, J_0(x)$ gives a central value of $J_0(0) = -3.49 \times 10^6$ Am^{-2}. Assumption of the static equilibrium conditions (7) gives a central safety factor of $q(0) = -1.25$ and an edge value of $q(1) = -3.74$. Figure 2(a) shows radial profiles for the current density $|J_0(x)|$ and safety factor $|q(x)|$.

The electron density profile is assumed to be parabolic in shape, satisfying $n_e(x) = n_e(0)[1 - 0.99x^2]$. The ion density profile is assumed to be given by the condition of electrical neutrality (9). The edge density is chosen to be non-zero and set to 1% of the central value, $n_e(1) = 0.01 n_e(0)$. This is done so as to keep the Alfvén speed (18) finite. Figure 2(b)

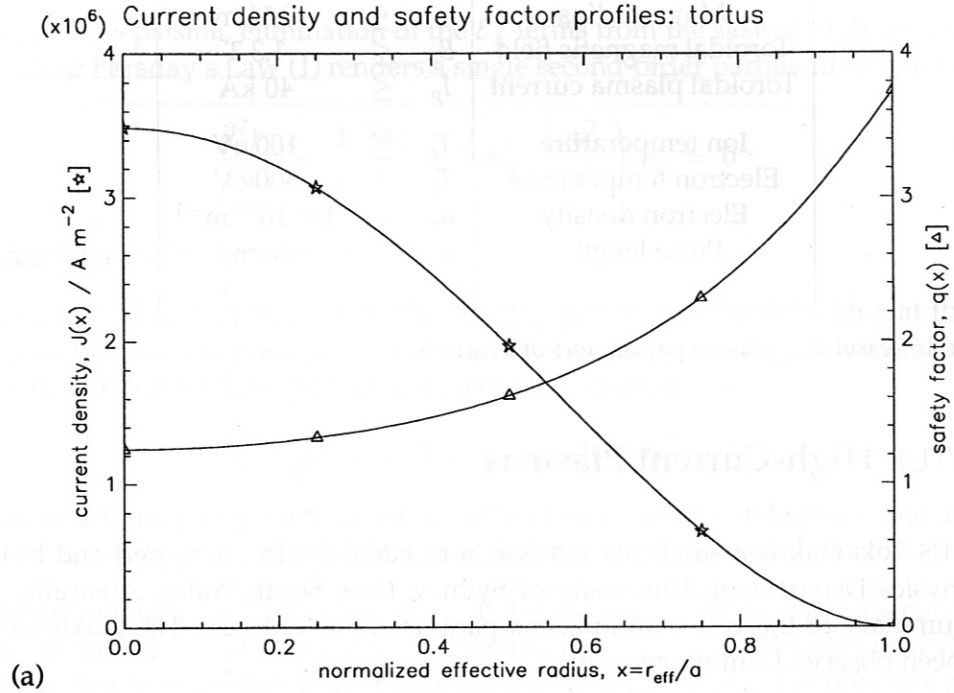

(a)

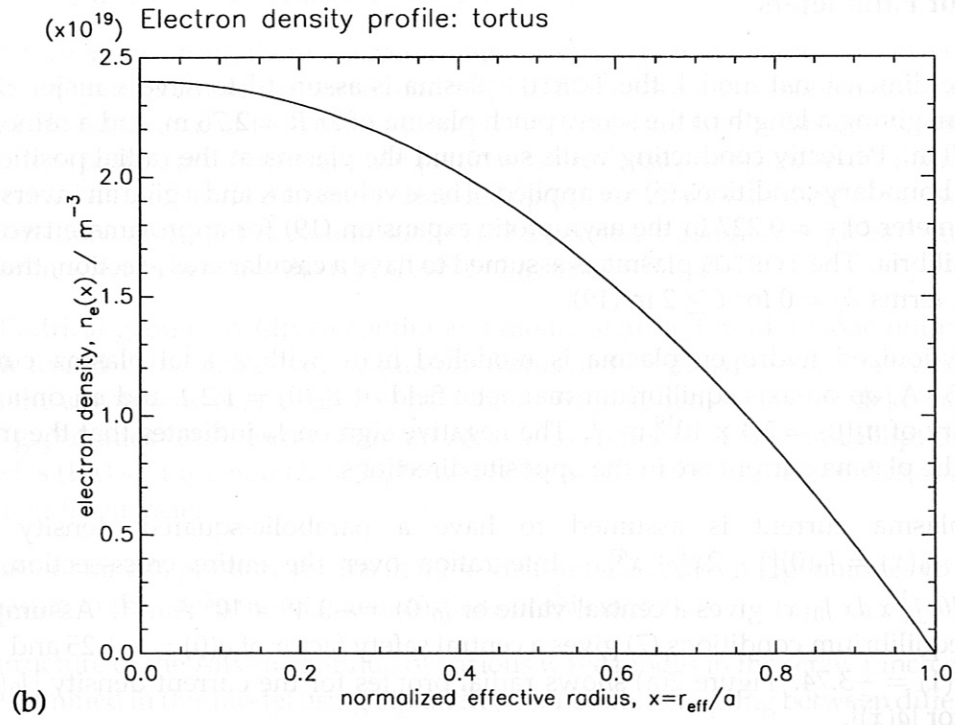

(b)

Figure 2: Equilibrium profiles used for the model of TORTUS plasmas: (a) the current density $|J_0(x)|$ [$\star$] and safety factor $|q(x)|$ [$\triangle$] profiles and (b) the electron density profile $n_e(x)$.

shows the electron density profile $n_e(x)$.

4.2 Alfvén Continuous Spectra

Figure 3 shows the Alfvén continua for modes with toroidal mode numbers $n = 0$, $n = 1$, $n = 2$ and $n = 3$. The radial position x is plotted on the horizontal axes, and the local Alfvén frequency $\omega_A(x)/2\pi$ on the vertical axes. The local Alfvén frequency at a particular layer $x = x_0$ corresponds to the frequency $\omega_A(x_0)$ at which the Alfvén resonance layer would occur at that radial position.

The graphs in the left column are cylindrical continua, calculated from the expression for the Alfvén resonance in cylindrical geometry (17), and the graphs in the right column show approximate two-dimensional continua, calculated from the asymptotic expansion (19). In the cylindrical continua, the m mode numbers are indicated on each dispersion curve. In these cylindrical (and cylindrical-like) calculations, the modes (m, n) and $(-m, -n)$, always share the same resonance layers.

The Alfvén continuum structure of the TORTUS plasma here is fairly typical for plasmas with relatively high shear in the $q(x)$ profile. There are, with the exception of the odd negative helicity mode or two, gaps below the lower edge of the Alfvén continuum only for modes with positive helicities. If the boundary conditions (5) can be satisfied at frequency inside this gap, a GAE with eigenfrequency $\omega_{GAE} < \min\{\omega_A(x)\}$ the corresponding (m, n) mode numbers will exist. Such GAE solutions will be discussed in the next section.

Negative helicity modes, on the other hand, have steep Alfvén continua which often extend down to zero frequency, $\omega_A(x_0) = 0$ at some $x_0 \in [0, 1]$. These modes tend to cross each other at some point in the plasma cross-section. Toroidal coupling leads to avoided crossings and gaps opening where neighbouring continua couple to each other. In this model where $\psi_\ell = 0$ for all $\ell \geq 2$, the only gap which opens is the TAE gap between the modes (m, n) and $(m + 1, n)$. EAE gaps and gaps for higher-order non-cylindrical Alfvén eigenmodes do not appear.

The width of the TAE gaps is not very large. For example, the gap between the (-2,1) and (3,-1) modes at $x \approx 0.8$ has a width of $\delta\omega \approx 2\epsilon x_0 |k_{\|m}(x_0) v_A(x_0)| \approx 80$ kHz. The presence of this gap in the continuum does not automatically ensure the presence of a TAE. A TAE will occur only if different poloidal harmonics can couple to produce a global mode which satisfies the boundary conditions (5), with a frequency in this gap $\omega_{TAE} \in (\omega_0 - \delta\omega, \omega_0 + \delta\omega)$. Conversely, several discrete TAE may also occur in this gap, should the boundary conditions be satisfied by several discrete eigensolutions.

Figure 3: (overleaf) Alfven continua for TORTUS. The graphs in the left column show the cylindrical continuum layers, those in the right column show the approximate two-dimensional coupled continuum layers. Separate graphs are plotted for different n numbers, and m numbers are marked close to the start of the curves.

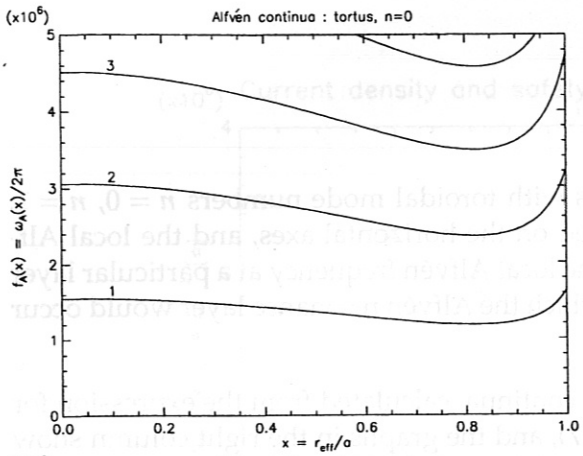
(x10^6)
Alfvén continua : tortus, n=0
3
2
1
f_A(x) = ω_A(x)/2π
x = r_eff/a

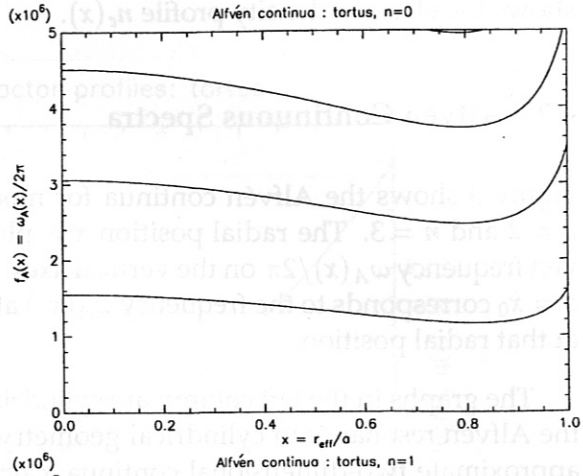
(x10^6)
Alfvén continua : tortus, n=0
f_A(x) = ω_A(x)/2π
x = r_eff/a

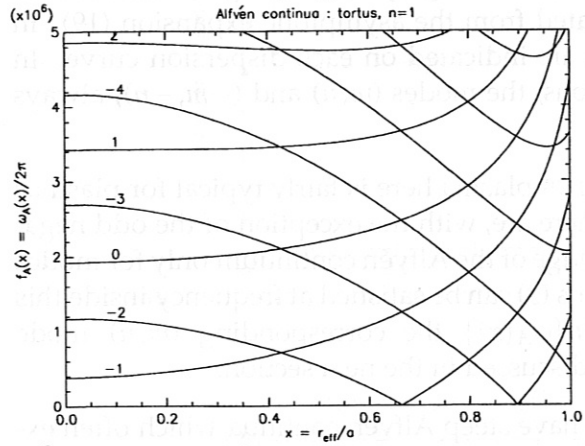
(x10^6)
Alfvén continua : tortus, n=1
2
-4
1
-3
0
-2
-1
f_A(x) = ω_A(x)/2π
x = r_eff/a

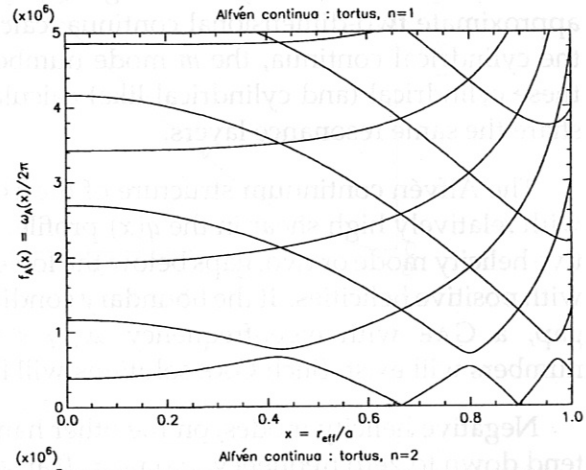
(x10^6)
Alfvén continua : tortus, n=1
f_A(x) = ω_A(x)/2π
x = r_eff/a

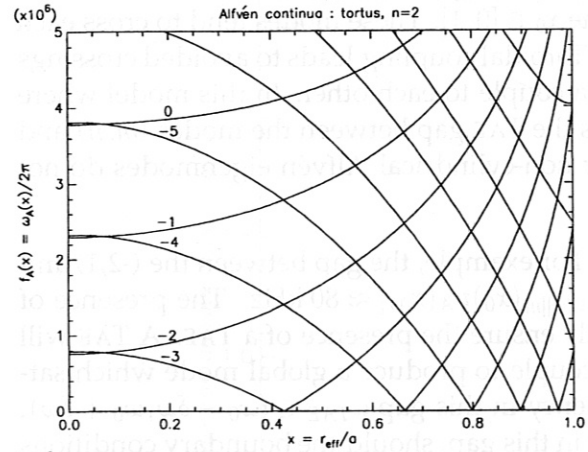
(x10^6)
Alfvén continua : tortus, n=2
0
-5
-1
-4
-2
-3
f_A(x) = ω_A(x)/2π
x = r_eff/a

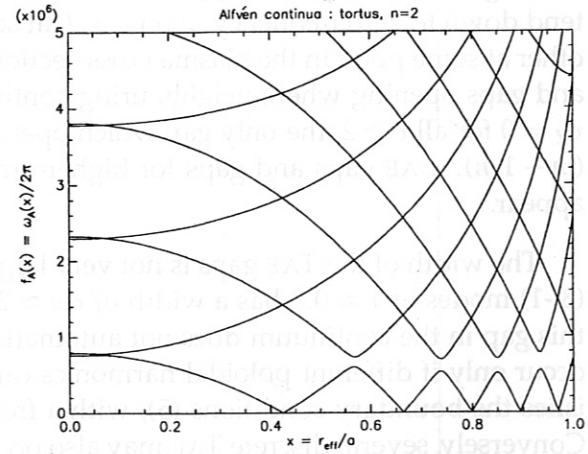
(x10^6)
Alfvén continua : tortus, n=2
f_A(x) = ω_A(x)/2π
x = r_eff/a

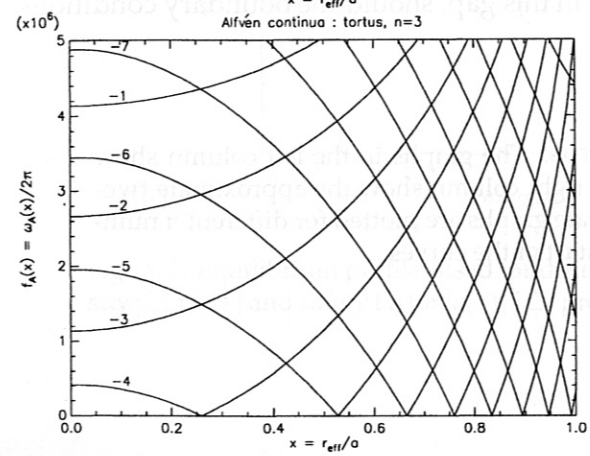
(x10^6)
Alfvén continua : tortus, n=3
-7
-1
-6
-2
-5
-3
-4
f_A(x) = ω_A(x)/2π
x = r_eff/a

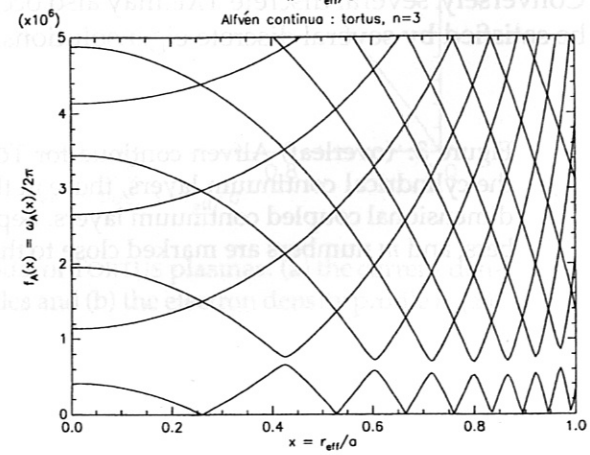
(x10^6)
Alfvén continua : tortus, n=3
f_A(x) = ω_A(x)/2π
x = r_eff/a

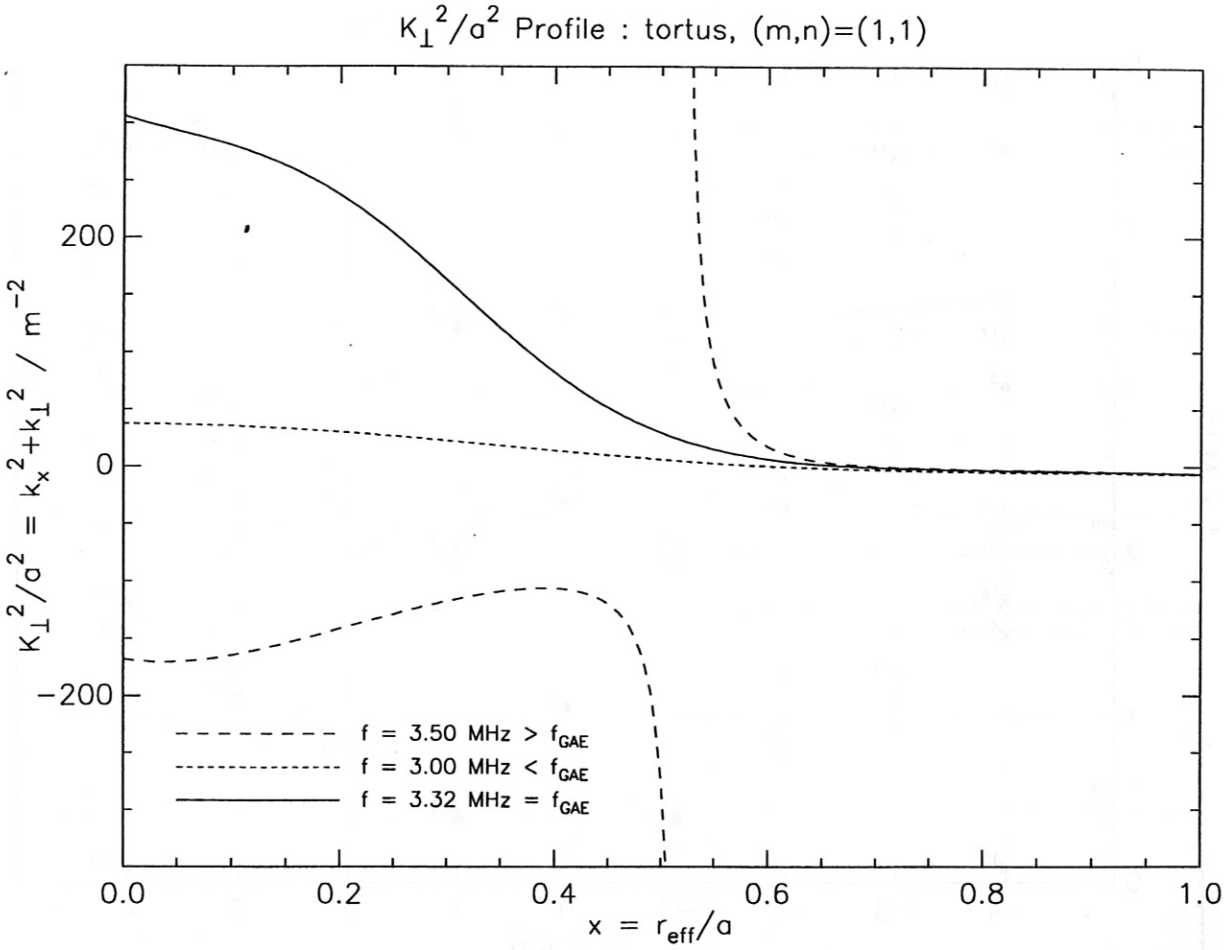

Figure 4: The radial profile of the K_Λ^2 parameter for the (1,1) mode in TORTUS. Three profiles are shown for waves at different frequencies, one at the GAE resonance frequency, one at a frequency below the lower edge of the Alfvén continuum and one at a frequency within the Alfvén continuum.

4.3 Discrete GAE Solutions

The radial profile of the non-parallel wave vector K_Λ^2 is shown for the (1,1) mode in Figure 4. Three radial profiles are shown, for a frequency well below the lower edge of the Alfvén continuum frequency of this mode ($\min\{f_A(x)\} = 3.42$ MHz for this mode), at a frequency within the Alfvén continuum and at a frequency just below this lower edge where a solution of the linearized wave dispersion relations (13) exists satisfying the boundary conditions (5). This solution of the eigensystem is interpreted as a GAE and will be discussed in the following paragraphs.

The curves in Figure 4 are typical for TORTUS Alfvén wave modes. At frequencies far below the Alfvén resonance, there is little propagation in either of the directions non-parallel to the magnetic field. If K_Λ^2 gets to be large over a significant proportion of the plasma radius, a global eigenmode of the Alfvén wave, satisfying the boundary conditions, can exist: a standing wave in both the radial and azimuthal directions is set up due to reflections at the vessel

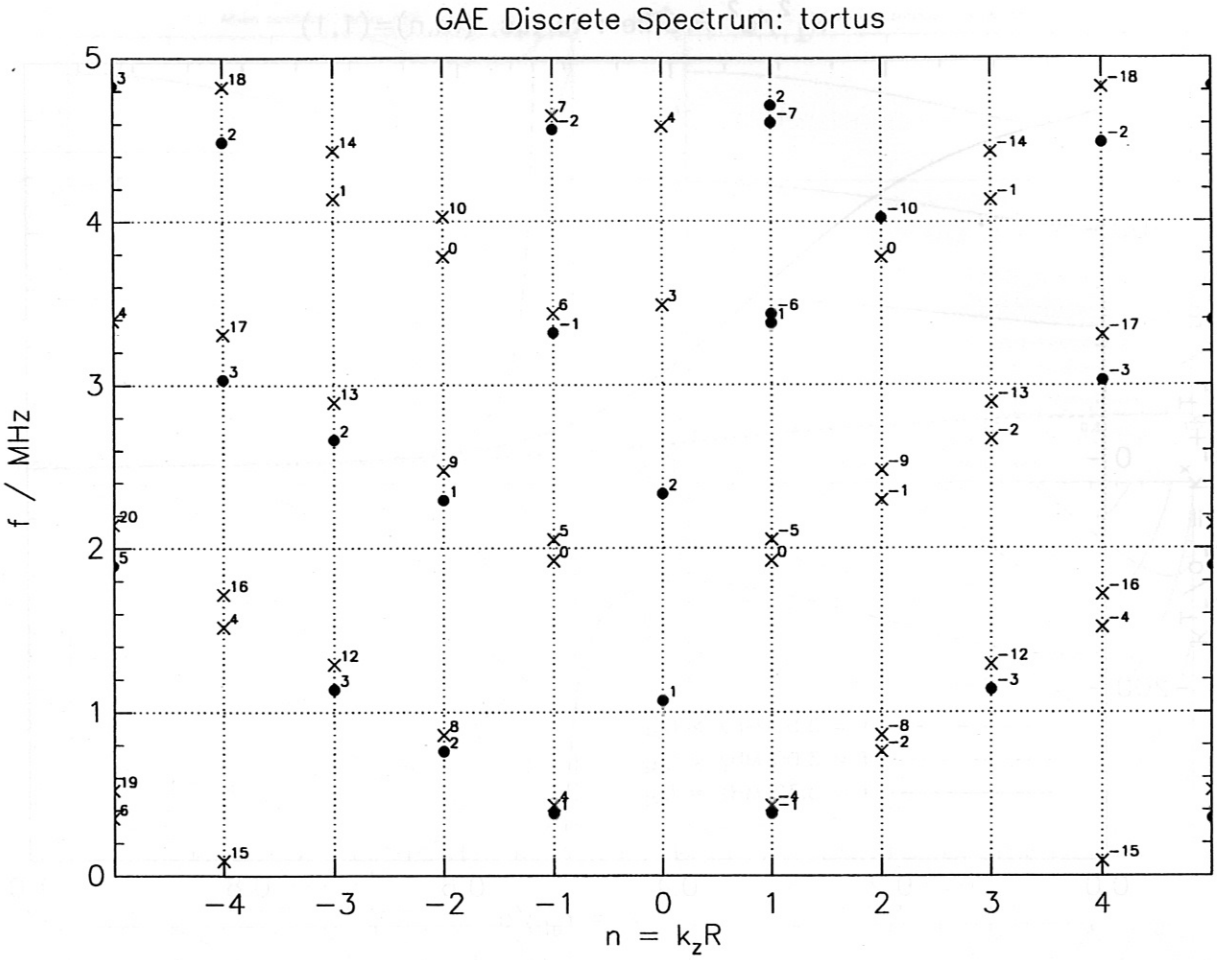

Figure 5: The discrete spectrum of GAEs in TORTUS. The mode n number is plotted on the horizontal axis and the mode m number is indicated on the graph. Modes with identified GAEs are marked with a dot (•), and where no GAE was found numerically, the lower edge of the Alfvén continuum is indicated with a cross (×).

walls, leading to a cavity resonance. Typically, these global modes appear when the Alfvén resonance condition is *almost* satisfied over most of the plasma cross-section.

Moving a little further up in wave frequency, we run into the Alfvén continuum. At the wave frequency of $f = 3.50$ MHz shown in Figure 4, the Alfvén resonance condition (17) of the (1,1) mode is satisfied at the layer at a radial position of $x = 0.520$. At this layer, a logarithmic singularity occurs in the dispersion relation and the non-parallel wave vector $K_\Lambda \to \pm\infty$. Inclusion of wave damping into the model (eg. resistivity) would result in a finite value for K_Λ at this layer and a study of the wave dynamics reveals that the wave solution on the high-density side of the layer (in this case: the left-hand side) is a Fast Wave; and that on the low-density side is an Alfvén Wave. Mode conversion between these two wave modes at this layer manifests itself in the form of the Alfvén resonance.

A search for GAEs at frequencies below the lower edge of their corresponding Alfvén continua reveals a spectrum of GAEs in the TORTUS plasma. Figure 5 shows the discrete spec-

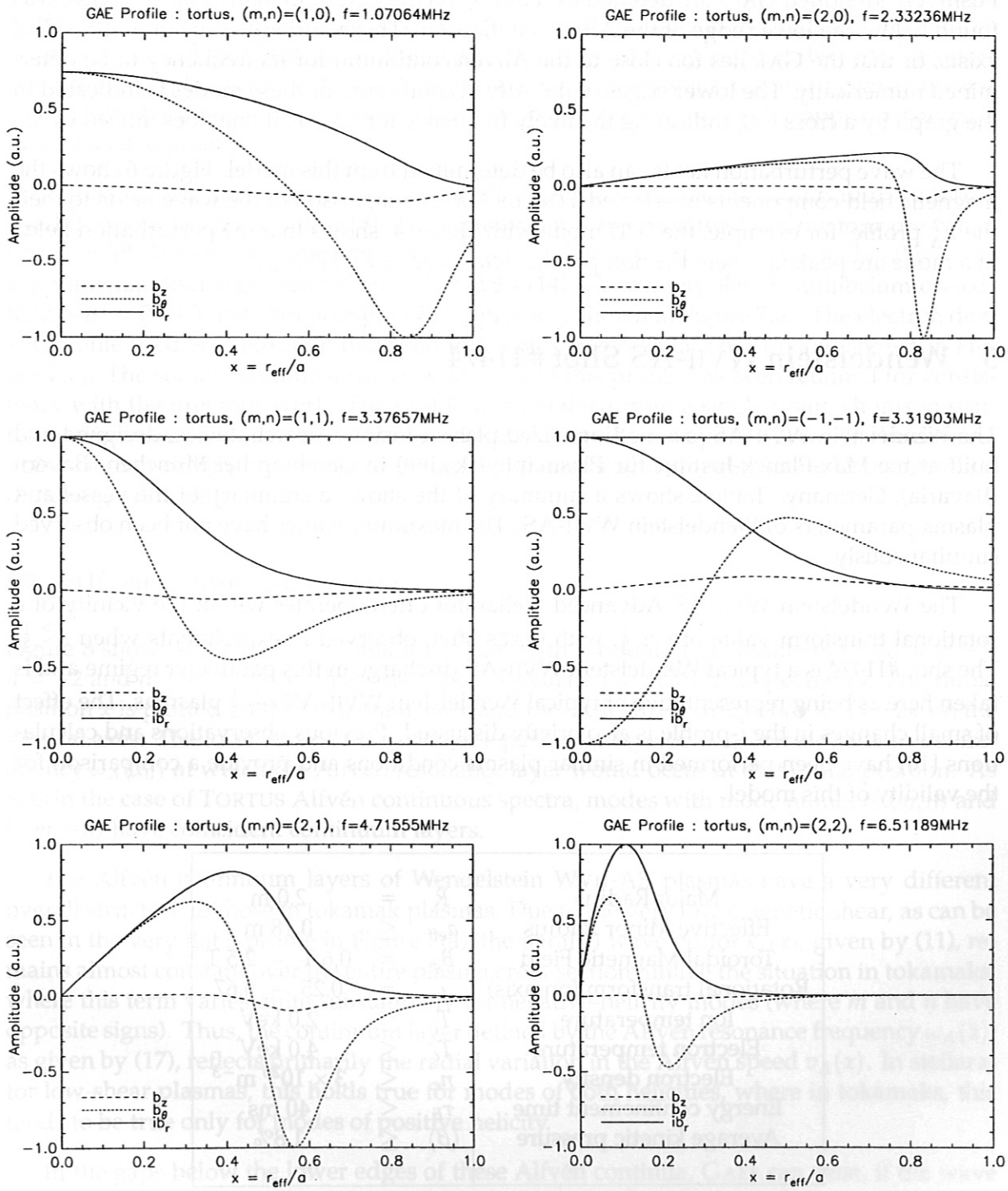

Figure 6: Wave perturbation magnetic fields of selected TORTUS GAEs.

trum of GAEs in TORTUS, where the wave frequency is plotted on the vertical axis, the mode n number is plotted on the horizontal axis and the wave m number is indicated on the graph. Positively identified GAEs are denoted by a dot (•) on the graph. In many cases, no GAE was found below the lower edge of the Alfvén continuum. This could either mean that no GAE exists, or that the GAE lies too close to the Alfvén continuum for its frequency to be determined numerically. The lower edges of the Alfvén continuum of these modes is indicated in the graph by a cross (×), indicating the likely frequency for a GAE, if one does indeed exist.

The wave perturbation fields can also be determined from this model. Figure 6 shows the magnetic field components of selected TORTUS GAE. Comparison of the wave fields to their the K_Λ^2 profile, for example, the (1,1) mode with Figure 4, shows that the perturbation fields of a mode are peaked where the non-parallel wave vector K_Λ^2 is large.

5 Wendelstein WVII-AS Shot #11474

The Wendelstein WVII-AS is a medium-sized plasma fusion research device, designed and built at the Max-Planck-Institut für Plasmaphysik (IPP) in Garching bei München, Bayern (Bavaria), Germany. Table 2 shows a summary of the shows a summary of the vessel and plasma parameters of Wendelstein WVII-AS. The maximum values have not been observed simultaneously.

The Wendelstein WVII-AS Advanced Stellarator often operates within the vicinity of a rotational transform value of $\iota \approx \frac{1}{3}$, with GAEs often observed in experiments when $\iota \gtrsim \frac{1}{3}$. The shot #11474 is a typical Wendelstein WVII-AS discharge in this parameter regime and is taken here as being representative of typical Wendelstein WVII-AS $\iota \gtrsim \frac{1}{3}$ plasmas. The effect of small changes in the ι-profile is also briefly discussed. Previous observations and calculations [10] have been performed in similar plasma conditions and provide a comparison for the validity of this model.

Major Radius	R	=	2.0 m
Effective Minor Radius	a_{eff}	$\leq$	0.18 m
Toroidal Magnetic Field	B_ϕ	=	0.6 T – 2.5 T
Rotational transform (on-axis)	ι	=	0.25 – 0.67
Ion temperature	T_i	$\leq$	2.0 keV
Electron temperature	T_e	$\leq$	4.0 keV
Electron density	n_e	$\leq$	3×10^{20} m^{-3}
Energy confinement time	τ_E	$\leq$	40 ms
Average kinetic pressure	$\langle\beta\rangle$	$\leq$	1.8%

Table 2: Plasma parameters of Wendelstein WVII-AS.

5.1 Input Parameters

In this one-dimensional model, the Wendelstein WVII-AS plasma is assumed to have a major radius of $R = 2.00$ m, giving a length of the screw pinch plasma of $2\pi R = 12.6$ m, and a minor radius of $a = 0.18$ m. Perfectly conducting walls surround the plasma at the radial position $r = a$, where the boundary conditions (5) are applied. These values of R and a give an inverse aspect ratio parameter of $\epsilon = 0.090$ in the asymptotic expansion (19) for approximate two-dimensional equilibria.

A fully-ionized hydrogen plasma is modelled here, and the plasma equilibrium is interpolated from the TRANS database [9]. The equilibrium is interpolated from the four pre-calculated equilibria in this database whose parameters lie closest to the settings used in the actual experimental discharge Wendelstein WVII-AS #11474. The interpolated equilibrium on-axis field is $B_0 = 2.54$ T and the corresponding q-profile is shown in Figure 7(a). The electron density profile used is identical to that used in the previous calculations [10] and shown in Figure 7(b). The somewhat unrealistic cusp at $x = 0$ in this profile has been retained for consistency with the previous work. The profile was obtained from a single-point Thomson scattering diagnostic over a series of almost identical shots. To interpolate between the discrete points, fourth-order polynomials were fitted to them using a Singular Value Decomposition (SVD) algorithm [8].

5.2 Alfvén Continuous Spectra

Figure 8 shows the Alfvén continua for modes with toroidal mode numbers $n = 0$, $n = -1$, $n = -2$ and $n = -3$. These curves have been calculated in cylindrical geometry. The radial position x is plotted on the horizontal axes, and the local Alfvén frequency $\omega_A(x)/2\pi$ on the vertical axes. The local Alfvén frequency at a particular layer $x = x_0$ corresponds to the frequency $\omega_A(x_0)$ at which the Alfvén resonance layer would occur at that radial position. As was in the case of TORTUS Alfvén continuous spectra, modes with mode numbers (m, n) and $(-m, -n)$ have coincident continuum layers.

The Alfvén continuum layers of Wendelstein WVII-AS plasmas have a very different overall structure to those in tokamak plasmas. Due to the very low magnetic shear, as can be seen in the very flat q-profile in Figure 7(a), the parallel wave vector $k_\parallel(x)$, given by (11), remains almost constant over the entire plasma cross-section, unlike the situation in tokamaks, where this term varies quite substantially for negative-helicity modes (where m and n have opposite signs). Thus, the continuum layer defined by the Alfvén resonance frequency $\omega_A(x)$, as given by (17), reflects primarily the radial variation in the Alfvén speed $v_A(x)$. In stellarator low-shear plasmas, this holds true for modes of both helicities, where in tokamaks, this tends to be true only for modes of positive helicity.

In the gaps below the lower edges of these Alfvén continua, GAEs can exist, if the wave dispersion relations have an eigensolution which satisfies the boundary conditions (5). Such GAE solutions will be discussed in the next section.

The value of the $k_\parallel(x)$ term is much smaller for modes of negative helicity than for modes of positive helicity due to the opposing signs of m and n in (11). GAEs of negative helicity in stellarators have very low frequencies, much like TAEs in tokamaks, hence the danger that

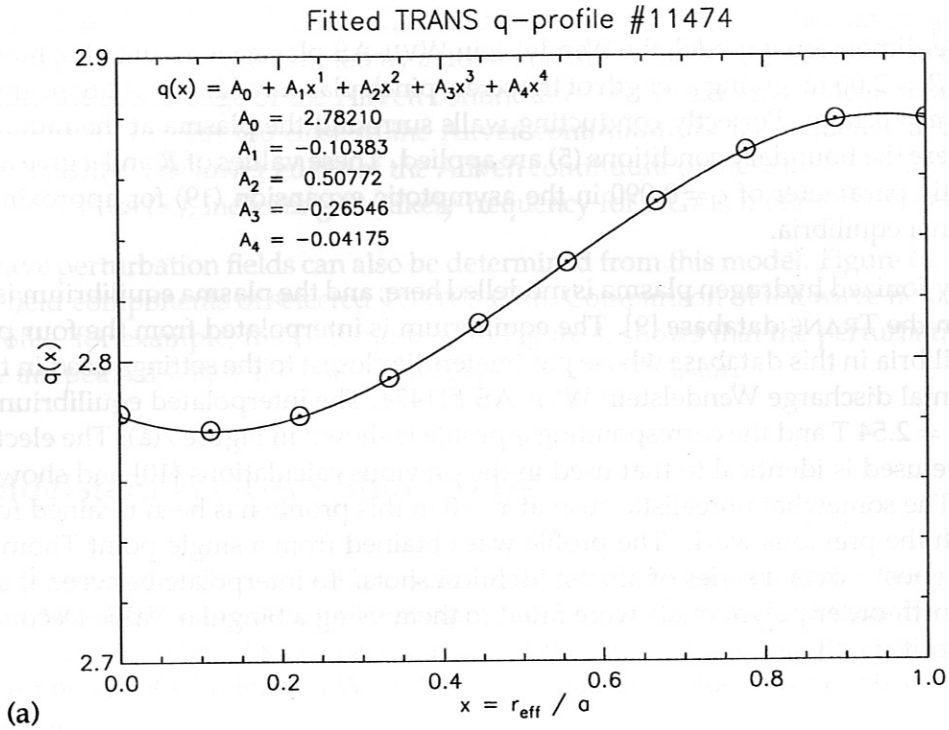

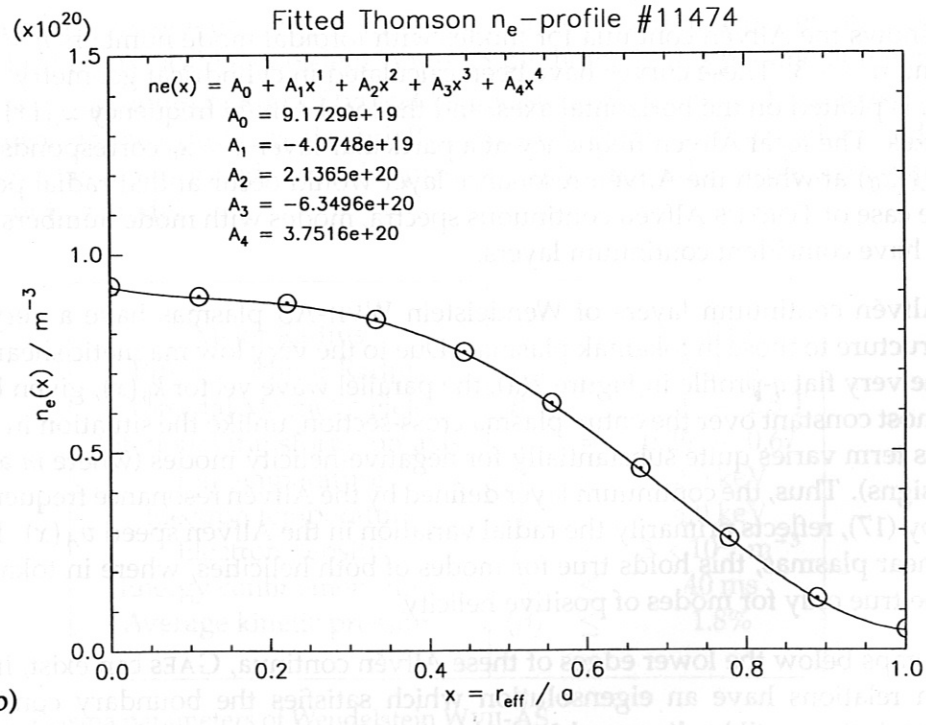

Figure 7: Equilibrium profiles used for the model of Wendelstein WVII-AS #11474. (a) The safety factor profile $q(x)$ and (b) the electron density profile $n_e(x)$. Fourth-order polynomials have been fitted to the discrete points.

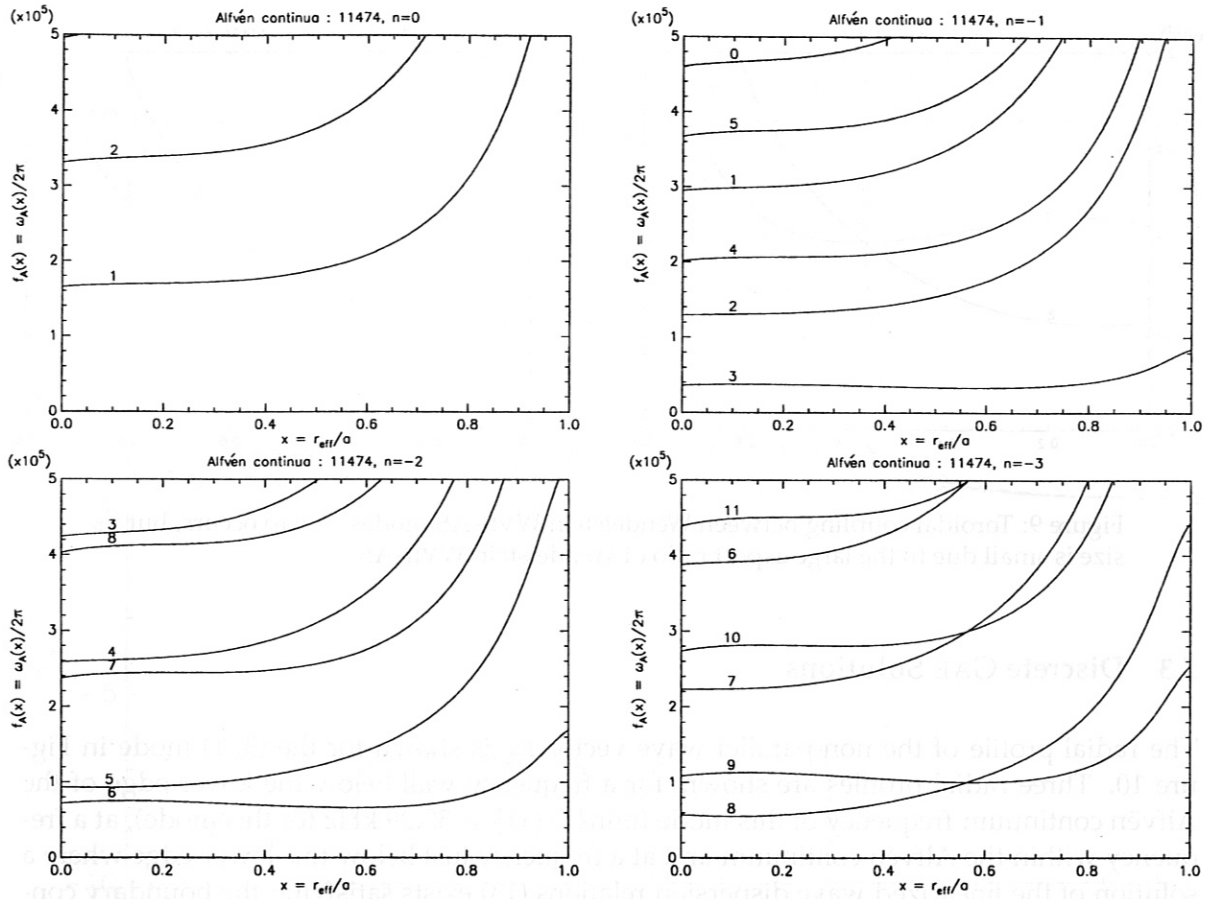

Figure 8: Alfvén continua for Wendelstein WVII-AS #11474. These curves have been calculated in cylindrical geometry and the curves for the $(m, -n)$ mode and the $(-m, n)$ mode are coincident.

they might be de-stabilized by energetic particles in the plasma. GAEs of positive helicity, like their tokamak counterparts, exist at much higher resonant frequencies, and are thus less likely to be destabilized.

Where the Alfvén continuum layers intersect each other, such as for the (8,-3) and (9,-3) modes in Figure 9 at $x = 0.71$ and $f_A = 124$ kHz, coupling between the modes in two-dimensional geometry may lead to the opening of gaps. The gap has been calculated using the asymptotic expansion (19) and is relatively small due to the large aspect ratio of Wendelstein WVII-AS.

As can be seen from the toroidal evolution of the Wendelstein WVII-AS plasma in Figure 7.3, the non-cylindrical terms ψ_ℓ/ψ_0 in the asymptotic expansion (19) will be of non-negligible amplitude for much larger values of ℓ than would be the case for a typical tokamak plasma. Approximate two-dimensional equilibria could be computed by taking some sort of "average" plasma cross-section.This will be further discussed in the next chapter, where a two-dimensional model is presented. The correct treatment of this problem would be to develop a three-dimensional model for the Alfvén continua.

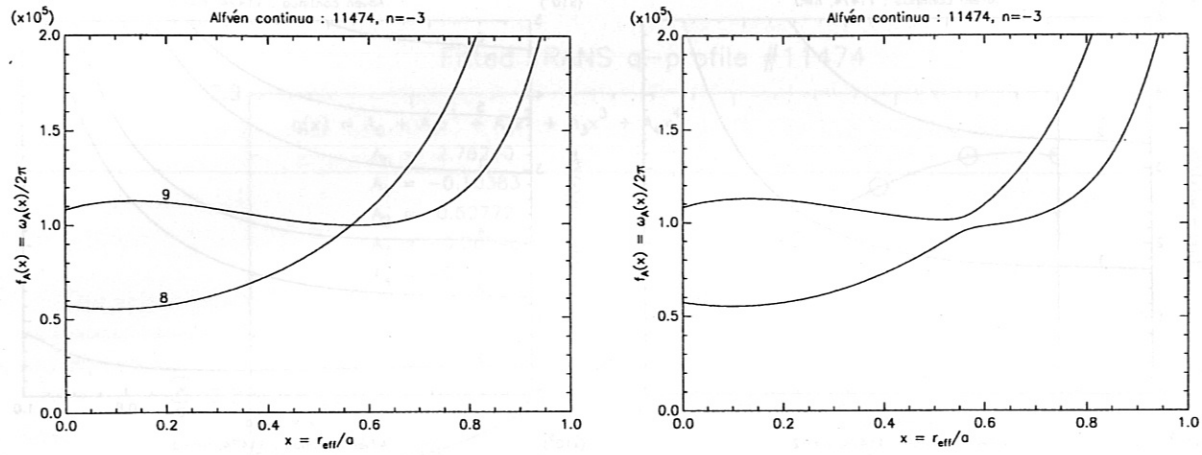

Figure 9: Toroidal coupling between Wendelstein WVII-AS modes. A gap occurs, but its size is small due to the large aspect ratio of Wendelstein WVII-AS.

5.3 Discrete GAE Solutions

The radial profile of the non-parallel wave vector K_Λ^2 is shown for the (3,-1) mode in Figure 10. Three radial profiles are shown, for a frequency well below the lower edge of the Alfvén continuum frequency of this mode ($\min\{f_A(x)\} = 33.29$ kHz for this mode), at a frequency within the Alfvén continuum and at a frequency just below this lower edge where a solution of the linearized wave dispersion relations (13) exists satisfying the boundary conditions (5). This solution of the eigensystem is interpreted as a GAE and will be discussed in the coming paragraphs.

These curves in Figure 10 are typical for Wendelstein WVII-AS Alfvén wave modes. As in the tokamak case, propagation is mostly parallel to the equilibrium magnetic field at frequencies far below the Alfvén resonance. Global eigenmodes of the Alfvén wave occur when K_Λ^2 gets to be large and the Alfvén resonance condition is *almost* satisfied over most of the plasma cross-section.

Moving a little further up in wave frequency, we run into the Alfvén continuum. At the wave frequency of $f = 34.00$ kHz shown in Figure 10(a), the Alfvén resonance condition (17) of the (3,-1) mode is satisfied at two layers in the plasma, at the radial position of $x = 0.465$ and $x = 0.671$, as shown in Figure 10(b). At these layers, logarithmic singularities occur in the dispersion relation and the non-parallel wave vector $K_\Lambda \to \pm\infty$. Inclusion of wave damping into the model (eg. resistivity) would result in a finite value for K_Λ at this layer and a study of the wave dynamics reveals that the wave solutions on the high-v_A sides of the layers (in this case: for $x < 0.465$ and $x > 0.671$) are Alfvén Waves; and that on the low-v_A sides ($0.465 < x < 0.671$) are Fast Waves. Mode conversion between these two wave modes at these layers manifests itself in the form of the Alfvén resonance.

Figure 11 shows the discrete GAE spectrum for Wendelstein WVII-AS #11474. The wave toroidal mode number n is plotted on the horizontal axis, the wave frequency on the vertical axis and the wave poloidal mode number m is labelled next to the points on the graph. As before, a search is carried out for a solution to the linearized wave dispersion relation (13),

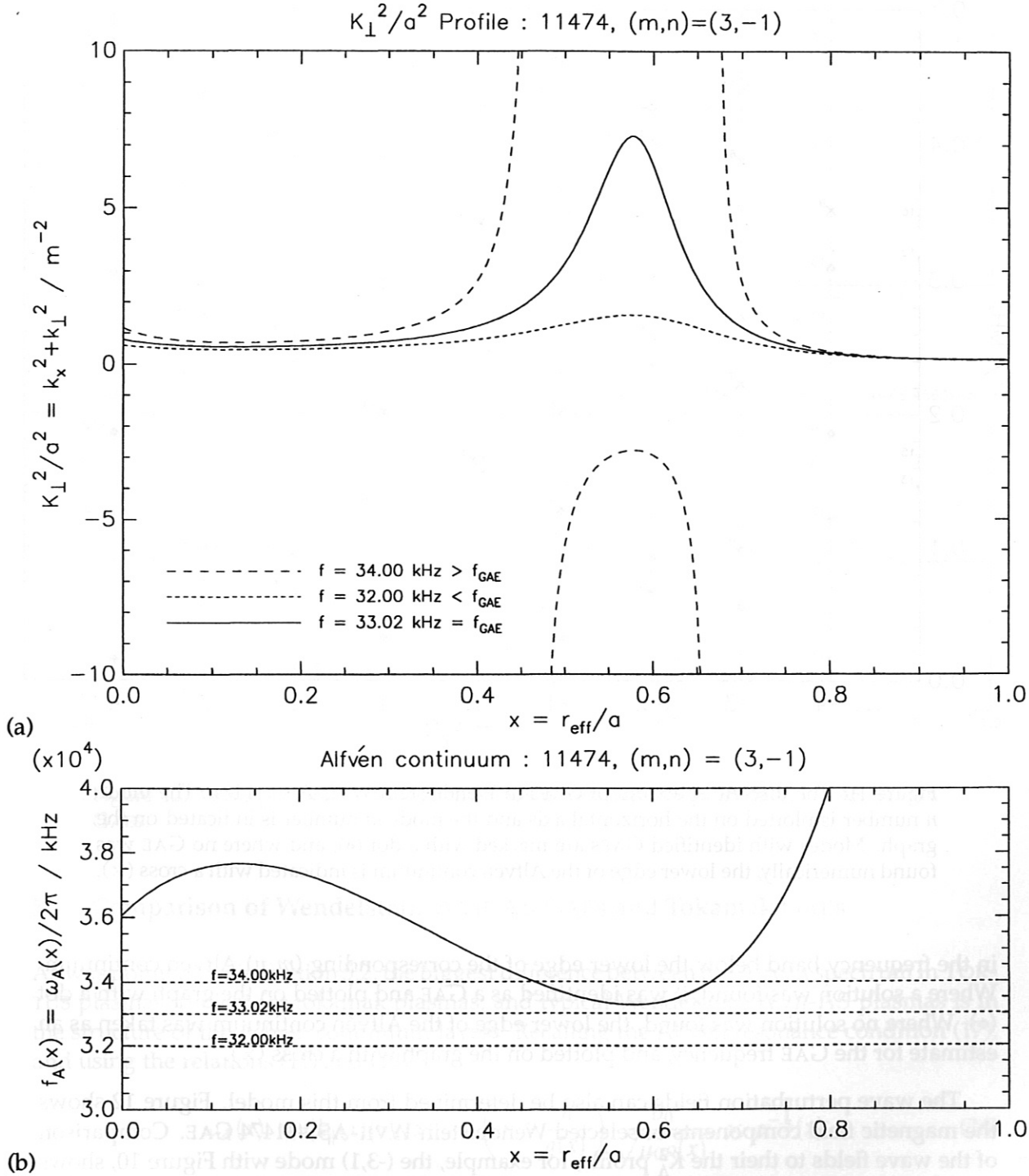

Figure 10: The radial profile of $\omega_A(x)$ and the K_Λ^2 parameter for the (3,-1) mode in Wendelstein WVII-AS #11474. Three profiles are shown for waves at different frequencies, one at the GAE resonance frequency, one at a frequency below the lower edge of the Alfvén continuum and one at a frequency within the Alfvén continuum.

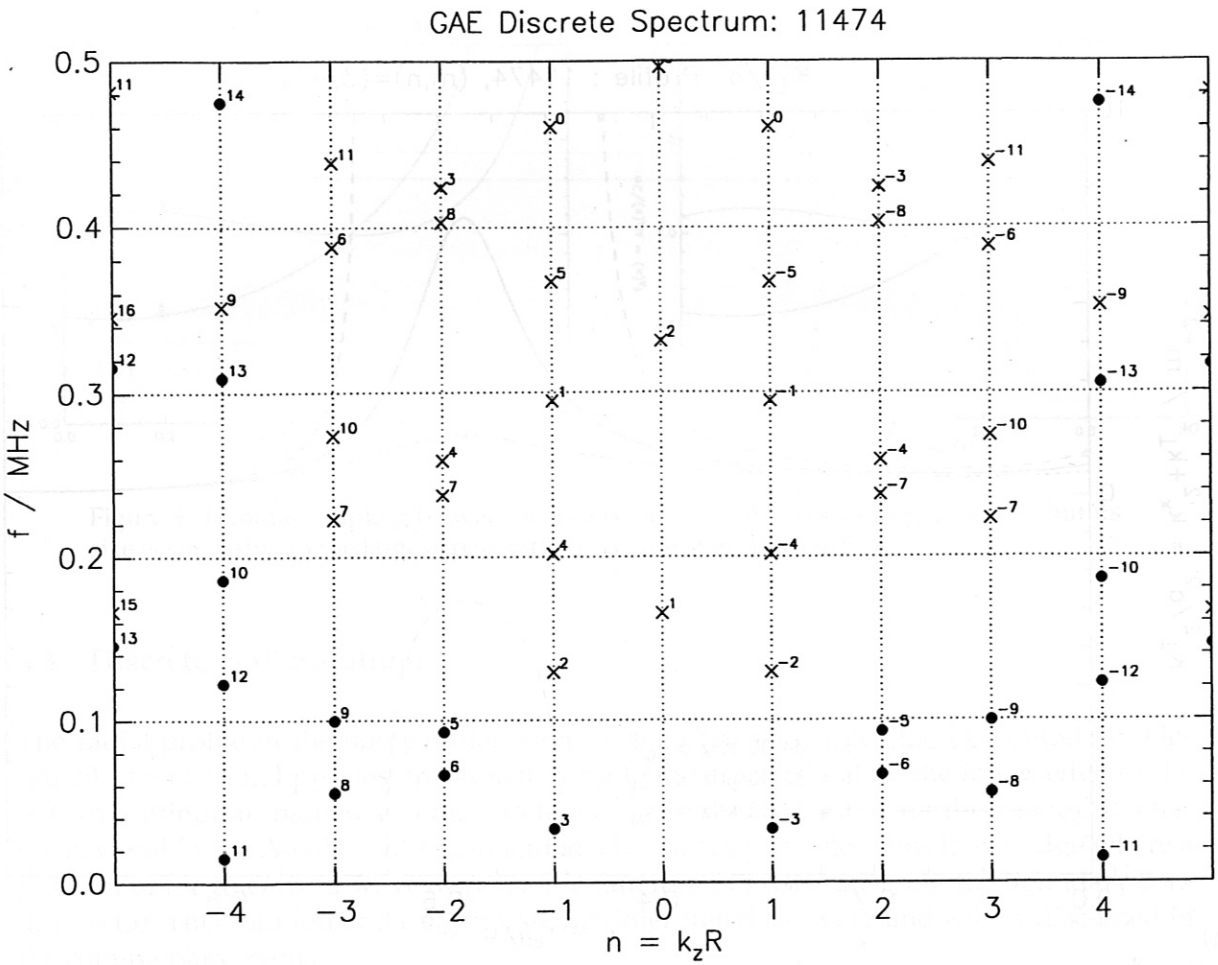

Figure 11: The discrete spectrum of GAEs in Wendelstein WVII-AS #11474. The mode n number is plotted on the horizontal axis and the mode m number is indicated on the graph. Modes with identified GAEs are marked with a dot (•), and where no GAE was found numerically, the lower edge of the Alfvén continuum is indicated with a cross (×).

in the frequency band below the lower edge of the corresponding (m,n) Alfvén continuum. Where a solution was found, it was identified as a GAE and plotted on the graph with a dot (•). Where no solution was found, the lower edge of the Alfvén continuum was taken as an estimate for the GAE frequency, and plotted on the graph with a cross (×).

The wave perturbation fields can also be determined from this model. Figure 12 shows the magnetic field components of selected Wendelstein WVII-AS #11474 GAE. Comparison of the wave fields to their the K_Λ^2 profile, for example, the (-3,1) mode with Figure 10, shows that the perturbation fields of a mode are peaked where the non-parallel wave vector K_Λ^2 is large.

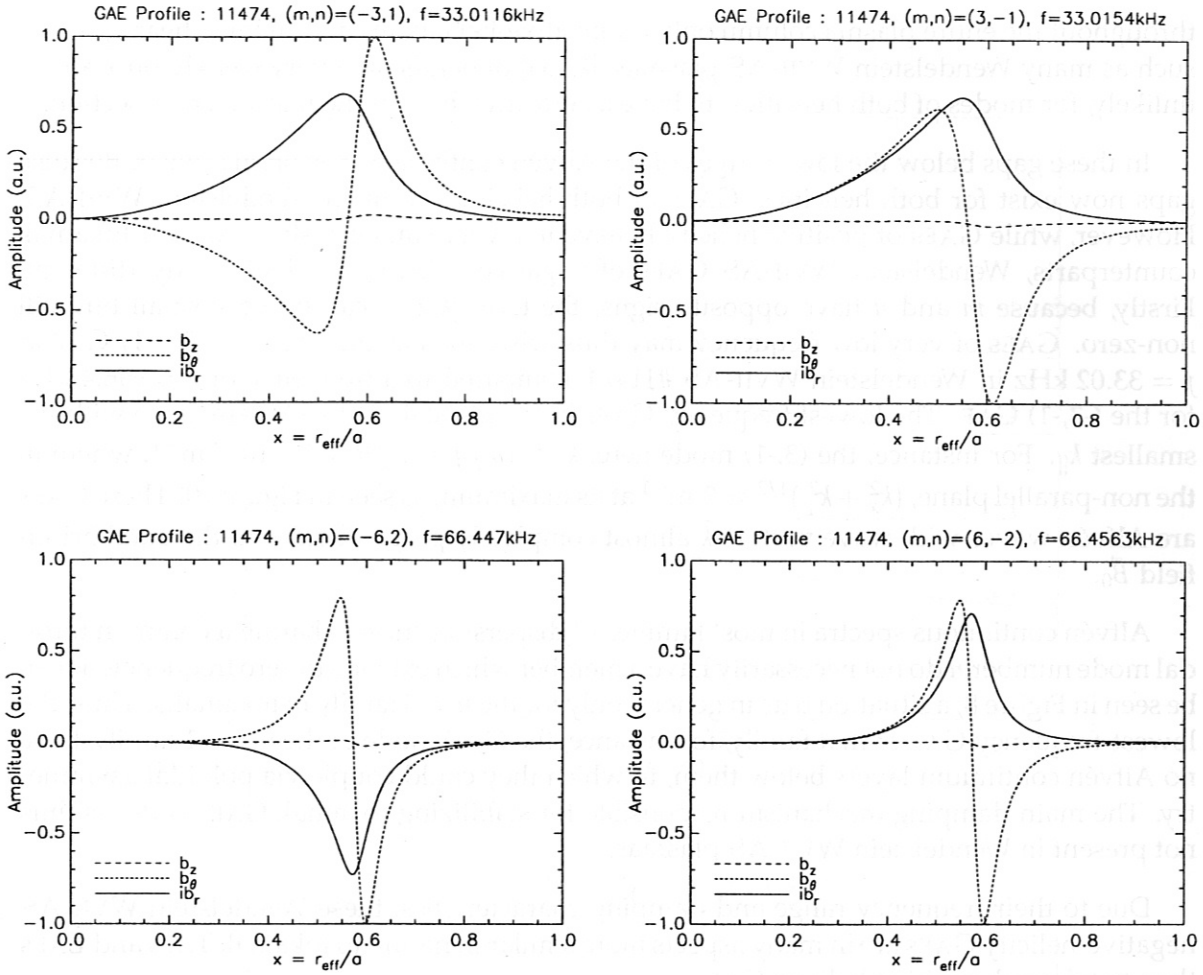

Figure 12: Wave perturbation magnetic fields of selected Wendelstein WVII-AS #11474 GAEs.

5.4 Comparison of Wendelstein WVII-AS GAEs and Tokamak GAEs

As was pointed out in Section 5.2, the biggest difference between the Alfvén spectrum in TORTUS plasmas, typical for tokamak plasmas, and typical Wendelstein WVII-AS plasmas is in the structure of the Alfvén continuum layers. Recalling the Alfvén resonance condition (17), and using the relations (11) and (18),

$$\omega_A(x) = |k_\parallel(x)| v_A(x) \approx \left(m + \frac{n}{q(x)}\right) \frac{B_0}{\sqrt{\mu_0 \rho(x)}} \propto \rho^{-\frac{1}{2}}(x) \tag{26}$$

if $q(x)$ remains close to being constant over the plasma cross-section, as is the case for the (3,-1) GAE in Wendelstein WVII-AS shot #11474.

The first consequence of this is that gaps now appear below the Alfvén continua for modes of both helicities, as can be seen by considering the parallel wave vector $|k_\parallel(x)|$. In high-shear systems, $|k_\parallel(x)|$ is a function strongly dependent on x and will, in the case of negative helicity modes, quite likely have a zero somewhere in the range $x \in [0,1]$; remaining non-zero

throughout the entire plasma column only for positive-helicity modes. In low-shear systems, such as many Wendelstein WVII-AS plasmas, $|k_{\|}(x)|$ depends only very weakly on x and is unlikely, for modes of both helicities, to have a zero anywhere in the plasma cross-section.

In these gaps below the lower edges of the Alfvén continua, GAEs often appear. Because gaps now exist for both helicities, GAEs of both helicities occur in Wendelstein WVII-AS. However, while GAEs of positive helicity behave in a very similar fashion to their tokamak counterparts, Wendelstein WVII-AS GAEs of negative helicity are significantly different. Firstly, because m and n have opposite signs, the term $|k_{\|}(x)|$ can be very small but still non-zero. GAEs of very low frequency may thus arise, such as the $(m,n) = (3,-1)$ GAE at $f = 33.02$ kHz in Wendelstein WVII-AS #11474; compared to a frequency of $f = 956.4$ kHz for the (-3,-1) GAE. The lowest frequency GAEs in Wendelstein WVII-AS are those with the smallest $k_{\|}$. For instance, the (3,-1) mode here, $k_{\|} \approx (m/q + n)/R \lesssim 2 \times 10^{-2}\ \mathrm{m}^{-1}$, where in the non-parallel plane, $(k_x^2 + k_\perp^2)^{1/2} \approx 7\ \mathrm{m}^{-1}$ at its maximum, as seen in Figure 10. These GAEs are Alfvén waves with wave vectors $\vec{k}$ almost completely perpendicular to the equilibrium field $\vec{B}_0$.

Alfvén continuous spectra in most families of dispersion curves sharing a common toroidal mode number n do not necessarily have a member which extends to zero frequency, as can be seen in Figure 8; a situation true in general only for the $n = 0$ family in tokamaks. Thus, the lowest-frequency GAE of that family, for instance, the (3,-1) mode of the $n = -1$ family, have no Alfvén continuum layers below them, to which they could couple via poloidal asymmetry. The main damping mechanism responsible for stabilizing tokamak GAE modes is thus not present in Wendelstein WVII-AS plasmas.

Due to their frequency range and damping characteristics, these Wendelstein WVII-AS negative-helicity GAEs are in many aspects more similar in nature to tokamak TAEs and EAEs than to tokamak positive-helicity GAEs.

Plasma waves can interact with particles in the plasma via resonant interactions. For instance, waves could transfer energy to particles via Landau damping, and particles to waves via inverse Landau damping. It is feared that these low-frequency global eigenmodes of the Alfvén wave could be destabilized by fast particles, such as fusion-born α-particles and NBI ions. The wave modes could then trigger anomalous diffusion, affect the plasma equilibrium and lead to poor confinement of these fast particles. This would result in increased heat load on the vessel walls, plasma cooling and energy losses.

5.5 Effect of Small ι-Profile Variations

It has been experimentally observed that slight variations to the magnetic configuration can either change the frequency of a GAE or make it disappear altogether. Here, we perform a case study on the (3,-1) mode in Wendelstein WVII-AS #11474 to investigate this effect.

Figure 13(a) shows three ι-profiles returned by interpolation from the TRANS database. The profile used for modelling Wendelstein WVII-AS shot #11474 is shown, along with profiles for equilibria with ι-profiles lying respectively a little higher than and a little lower than the the #11474 profile. The rational surface at $\iota = \frac{1}{3}$ is indicated with a dotted line. TRANS does not return any equilibria containing low-order rational surfaces, so the equilibrium ly-

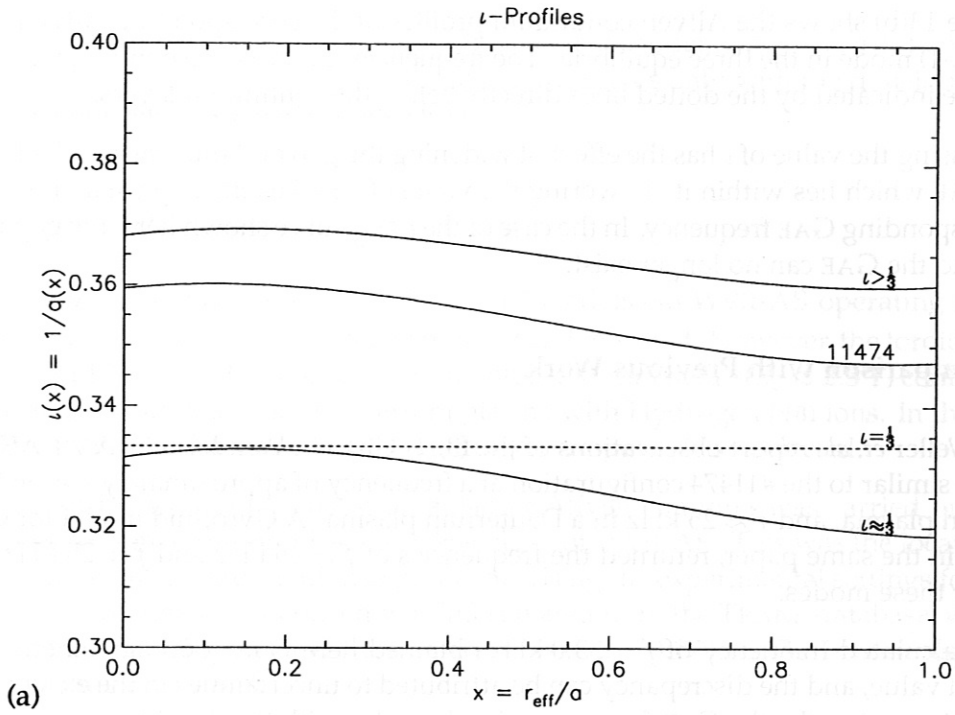

(a)

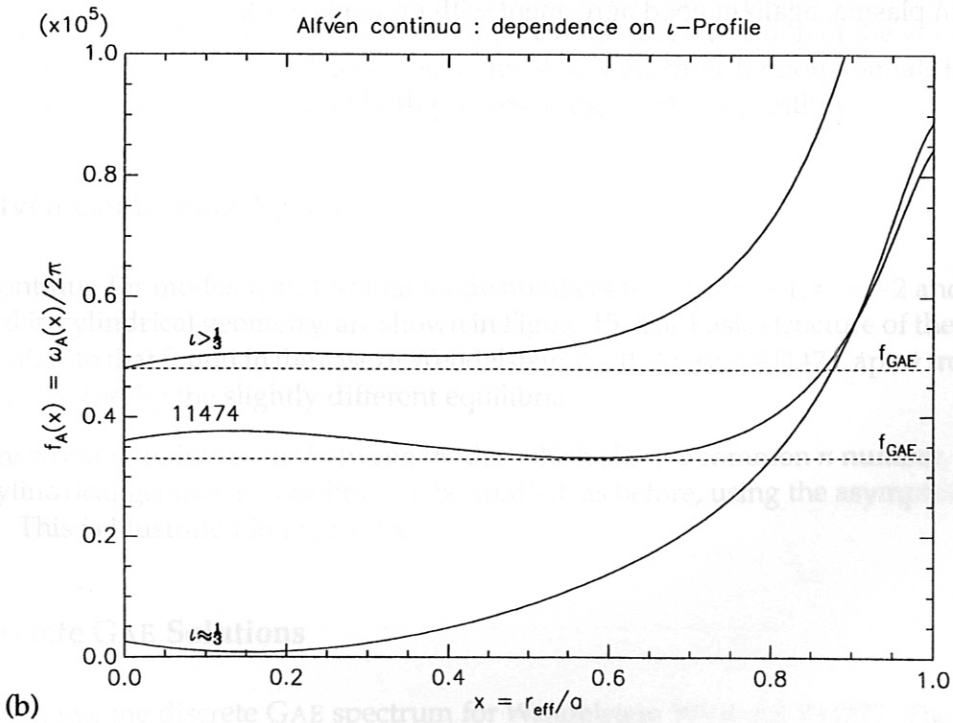

(b)

Figure 13: The effect of small ι-profile variations of the GAE gaps.

ing closest to $\iota = \frac{1}{3}$ was chosen.

Figure 13(b) shows the Alfvén continuum profiles of the corresponding Alfvén continua for the (3,-1) mode in the three equilibria. The frequencies of the corresponding GAEs, where found, are indicated by the dotted lines directly below the continuum layers.

Increasing the value of ι has the effect of widening the gap and thus raising the frequency of the GAE which lies within it. Lowering the value of ι makes the gap smaller and lowers the corresponding GAE frequency. In the case of the $\iota \approx \frac{1}{3}$ curve shown here, the gap virtually closes, and the GAE can no longer exist.

5.6 Comparison with Previous Work

In [10], Weller *et. al.* report observations of the (3,-1) GAEs in Wendelstein WVII-AS in plasmas very similar to the #11474 configuration at a frequency of approximately $f \approx 36$ kHz in a Hydrogen plasma, and $f \approx 25$ kHz in a Deuterium plasma. A Gyrofluid model for GAEs, as reported in the same paper, returned the frequencies of $f \approx 35$ kHz and $f \approx 25$ kHz, respectively, for these modes.

The calculated frequency of $f = 33.0$ kHz obtained here is in good agreement with the measured value, and the discrepancy can be attributed to uncertainties in the exact ι- and n_e-profiles. Assuming the the GAE frequency simply scales with the Alfvén speed v_A as given in (18), the model presented here predicts a frequency of $f = 23.3$ kHz for the (3,-1) GAE in a Deuterium plasma, again in good agreement with previous work.

6 Wendelstein WVII-AS Shot #34077

Having established the validity of the one-dimensional model, we now wish to apply it to an experimental situation. Here, we will concern ourselves only with the development of a model for Wendelstein WVII-AS shot #34077.

6.1 Input Parameters

The shot #34077 is, similar to shot #11474, in the Wendelstein WVII-AS operating regime of $\iota \gtrsim \frac{1}{3}$, where GAEs have previously been observed and reported. However, the toroidal field is in the "half field" ($B_0 \approx 1.25$ T) configuration unlike the "full field" ($B_0 \approx 2.5$ T) configuration of #11474, and the plasma was a Deuterium plasma with Hydrogen NBI ions. In this model, Z_{eff} is taken to be 2, and the effect of the Hydrogen "impurity" is neglected.

Analysis of mode coupling between adjacent Alfvén continua was carried out for the plasma cross-section at the elliptical ($\phi = 36^\circ$) plane of WVII-AS. This was the location of an antenna used for an active excitation experiment. Using the experimental settings for the coil currents, an approximate equilibrium was interpolated from the TRANS database, which has a major radius of $R = 2.114$ m and the minor radius of $a = 0.173$ m. The inverse aspect ratio parameter is thus $\epsilon = 0.0818$.

Figure 14 shows the q-profile returned with the interpolated equilibrium and the n_e-profile returned by a multichannel Thomson scattering diagnostic. The q-profile does not extend to the last closed flux surface, instead has been cut off at the radial position of the vessel's inner limiters, which determined the plasma size in this shot. Fourth-order polynomials have been fitted to the discrete points points in both profiles using an SVD algorithm.

6.2 Alfvén Continuous Spectra

Alfvén continua for modes with toroidal mode numbers $n = 0$, $n = -1$, $n = -2$ and $n = -3$, calculated in cylindrical geometry, are shown in Figure 15. The basic structure of the continua is very similar to that found in the case of Wendelstein WVII-AS shot #11474, apart from minor differences caused by the slightly different equilibria.

Where crossing points occur between modes which share a common n number, the effect of non-cylindrical geometric coupling can be studied, as before, using the asymptotic expansion (19). This is illustrated in Figure 16.

6.3 Discrete GAE Solutions

Figure 17 shows the discrete GAE spectrum for Wendelstein WVII-AS #34077. The wave toroidal mode number n is plotted on the horizontal axis, the wave frequency on the vertical axis and the wave poloidal mode number m is labelled next to the points on the graph. As before, a search is carried out for a solution to the linearized wave dispersion relation (13), in the frequency band below the lower edge of the corresponding (m, n) Alfvén continuum.

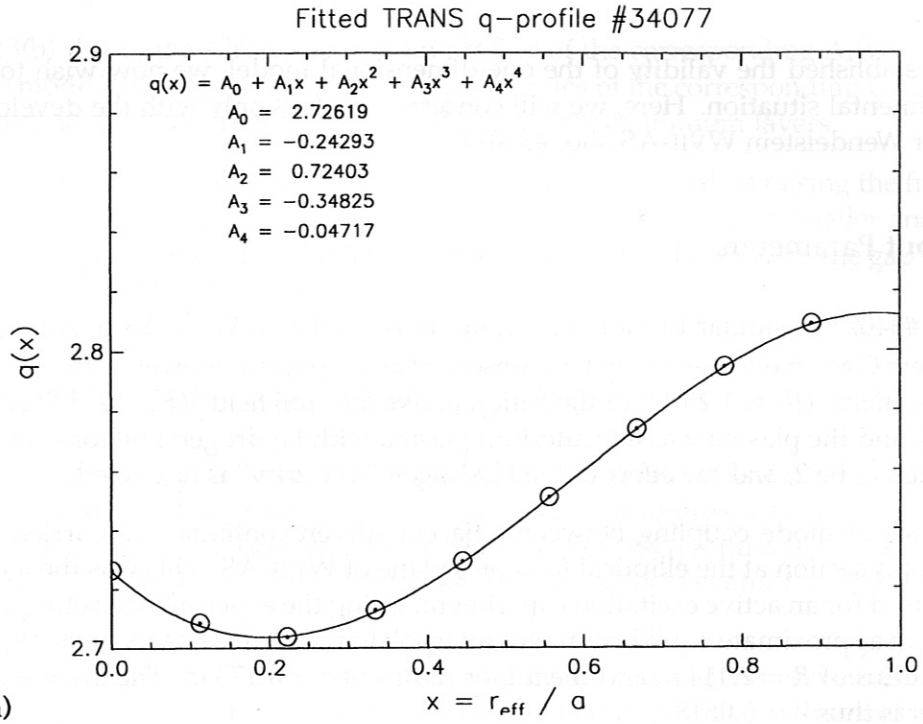

(a)

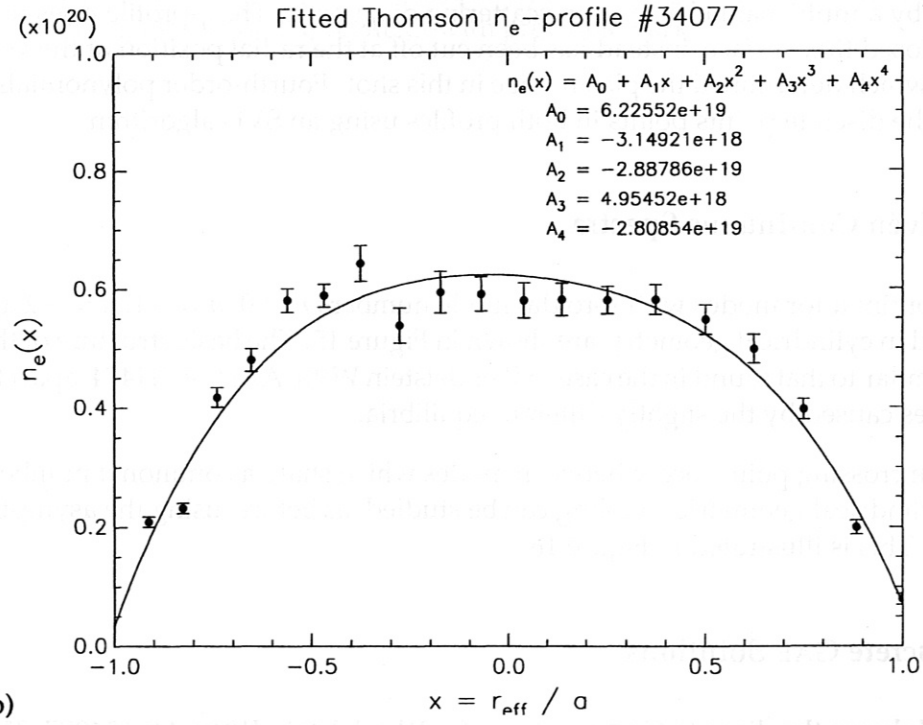

(b)

Figure 14: Equilibrium profiles used for the model of Wendelstein WVII-AS #34077. (a) The safety factor profile $q(x)$ and (b) the electron density profile $n_e(x)$. Fourth-order polynomials have been fitted to the discrete points.

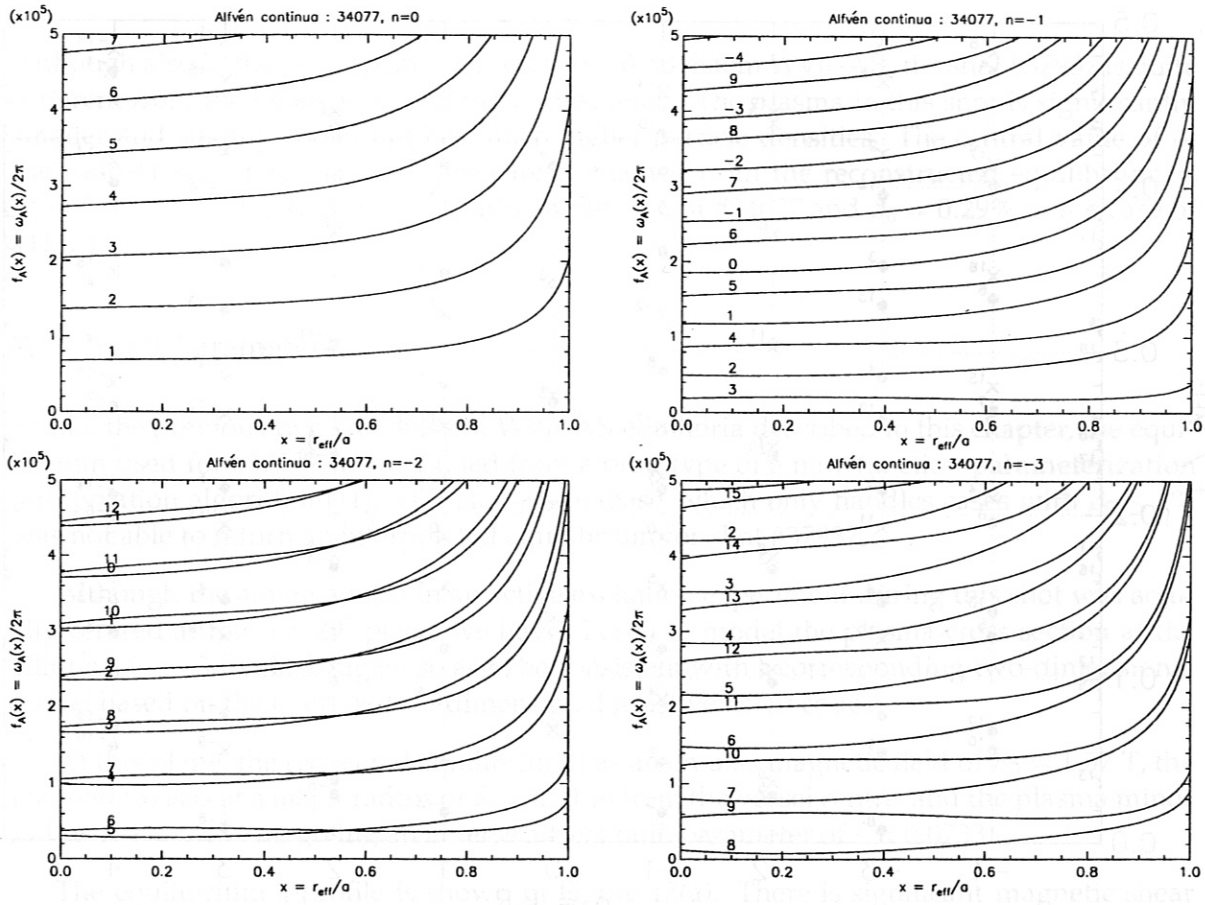

Figure 15: Alfvén continua for Wendelstein WVII-AS #34077. These curves have been calculated in cylindrical geometry and the curves for the $(m, -n)$ mode and the $(-m, n)$ mode are coincident.

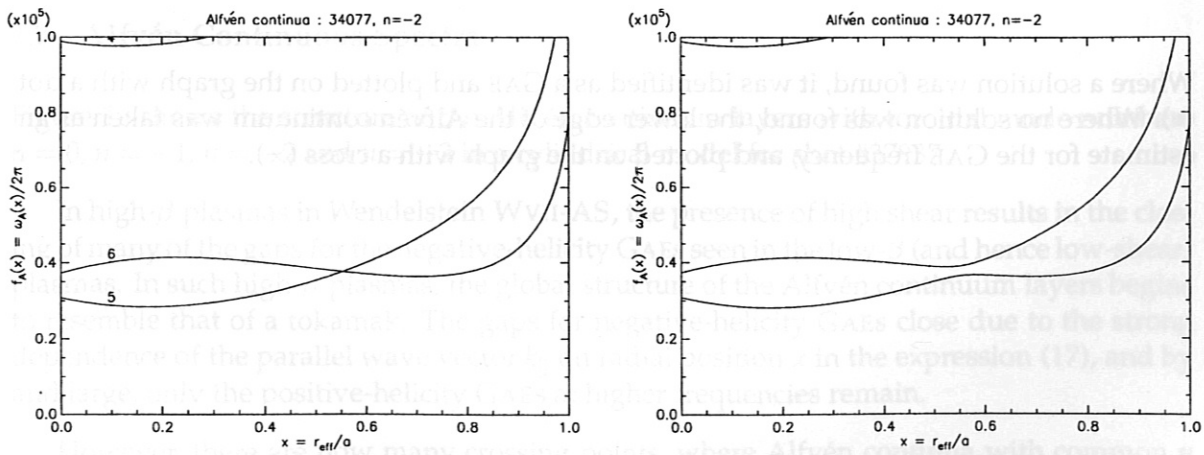

Figure 16: Toroidal coupling in Wendelstein WVII-AS #34077.

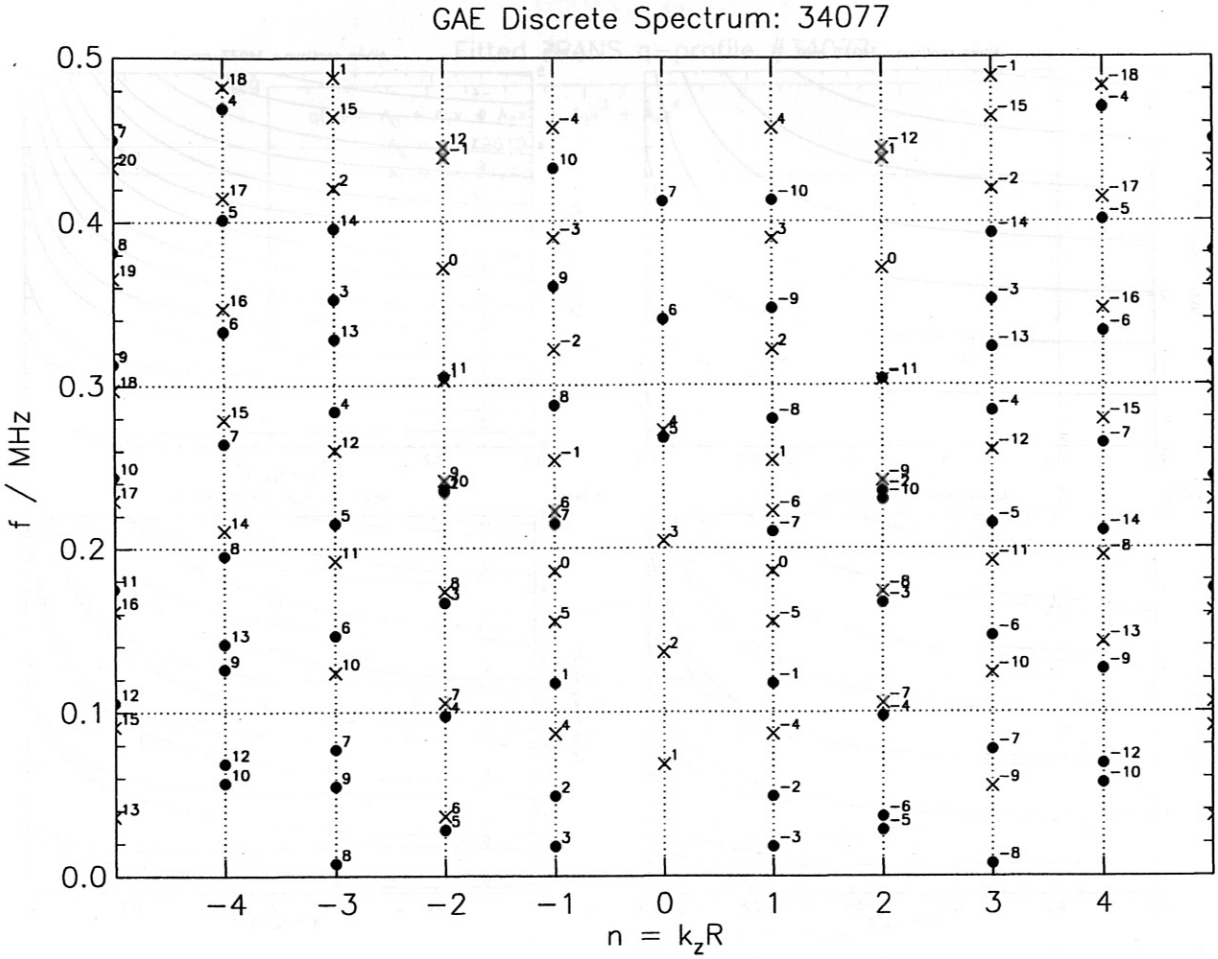

Figure 17: The discrete spectrum of GAEs in Wendelstein WVII-AS #34077. The mode n number is plotted on the horizontal axis and the mode m number is indicated on the graph. Modes with identified GAEs are marked with a dot (•), and where no GAE was found numerically, the lower edge of the Alfvén continuum is indicated with a cross (×).

Where a solution was found, it was identified as a GAE and plotted on the graph with a dot (•). Where no solution was found, the lower edge of the Alfvén continuum was taken as an estimate for the GAE frequency, and plotted on the graph with a cross (×).

7 Wendelstein WVII-AS Shot #37937

Although also in the $\iota \gtrsim \frac{1}{3}$ operating regime of Wendelstein WVII-AS, the shot #37937 is quite different from the other two previously considered. The plasma in this shot is significantly smaller and slightly cooler but has much higher particle densities. The central value of β, the ratio of kinetic to magnetic pressures, obtained from the reconstructed equilibrium is $\beta_0 = 2.39\%$, as compared to $\beta_0 = 0.40\%$ in the case of #34077 and $\beta_0 = 0.29\%$ in the case of #11474.

7.1 Input Parameters

Unlike the previous two Wendelstein WVII-AS equilibria described in this chapter, the equilibrium used for #37937 was obtained from a prototype of a new function parameterization interpolation algorithm [11]. The TRANS database, which only handles cases with $\beta_0 \leq 1\%$ was not able to return an interpolated equilibrium for shot #37937.

Although the antenna used in an active excitation experiment during this shot was actually centred at the $\phi = 29^\circ$ plane, we have chosen to model the plasma cross-section at the elliptical ($\phi = 36^\circ$) plane, again so as to be consistent with a corresponding two-dimensional model based on the CASTOR two-dimensional resistive MHD code.

At this plane, the recovered equilibrium has an on-axis magnetic field of $B_0 = 1.57$ T, the magnetic axis is at a major radius of $R = 2.11$ m from the vessel centre, and the plasma minor radius is $a = 0.154$ m, giving an inverse aspect ratio parameter of $\epsilon = 0.0733$.

The equilibrium q-profile is shown in Figure 18(a). There is significant magnetic shear here, compared to the previous low-β cases. Figure 18(b) shows the electron density profile, returned by the multichannel Thomson scattering diagnostic. The mass density profile is assumed to be given by the condition of quasi-neutrality (9) for a Deuterium plasma. As before, fourth order polynomials have been fitted to the discrete points in these profiles.

7.2 Alfvén Continuous Spectra

Figure 19 shows the structure of the Alfvén continuum layers with toroidal mode numbers $n = 0$, $n = -1$, $n = -2$ and $n = -3$ in a cylindrical model for shot #37937.

In high-β plasmas in Wendelstein WVII-AS, the presence of high shear results in the closing of many of the gaps for the negative-helicity GAEs seen in the low-β (and hence low-shear) plasmas. In such high-β plasmas, the global structure of the Alfvén continuum layers begins to resemble that of a tokamak. The gaps for negative-helicity GAEs close due to the strong dependence of the parallel wave vector $k_\parallel$ on radial position x in the expression (17), and by and large, only the positive-helicity GAEs at higher frequencies remain.

However, there are now many crossing points, where Alfvén continua with common n numbers cross each other in the cylindrical case. At these crossing points, the strongly non-cylindrically symmetric Wendelstein WVII-AS plasma is expected to give rise to gaps, such as the TAE gaps calculated with the asymptotic expansion (19) and plotted in Figure 20.

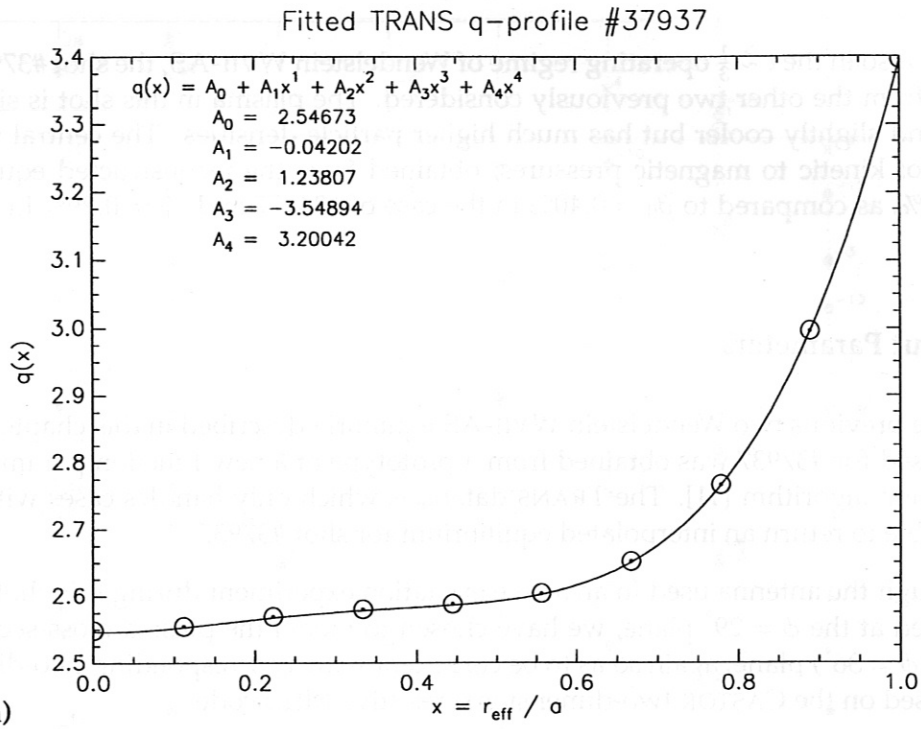

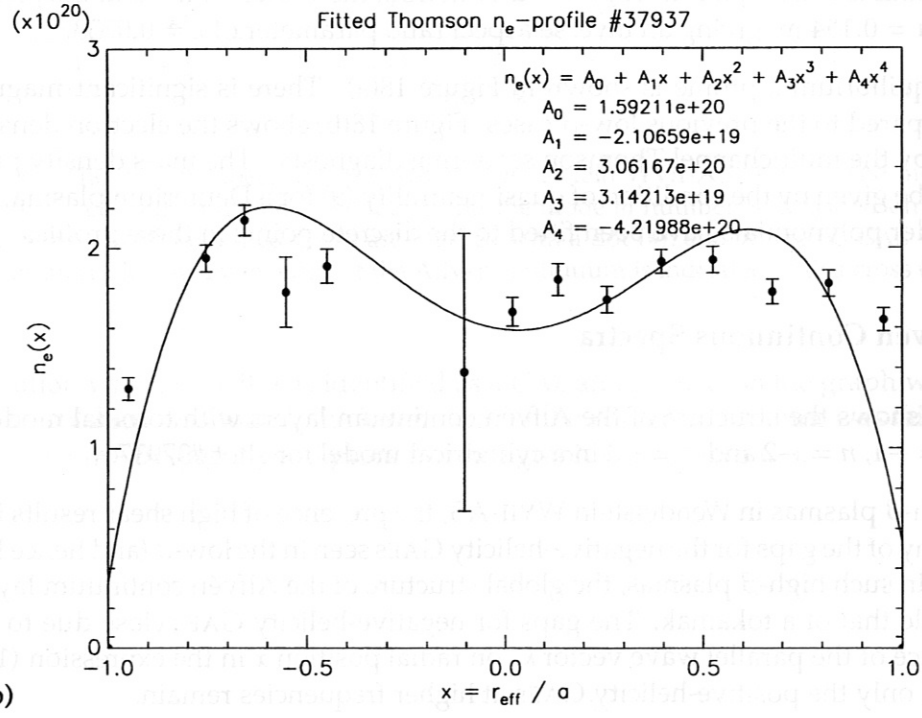

Figure 18: Equilibrium profiles used for the model of Wendelstein WVII-AS #37937. (a) The safety factor profile $q(x)$ and (b) the electron density profile $n_e(x)$. Fourth-order polynomials have been fitted to the discrete points.

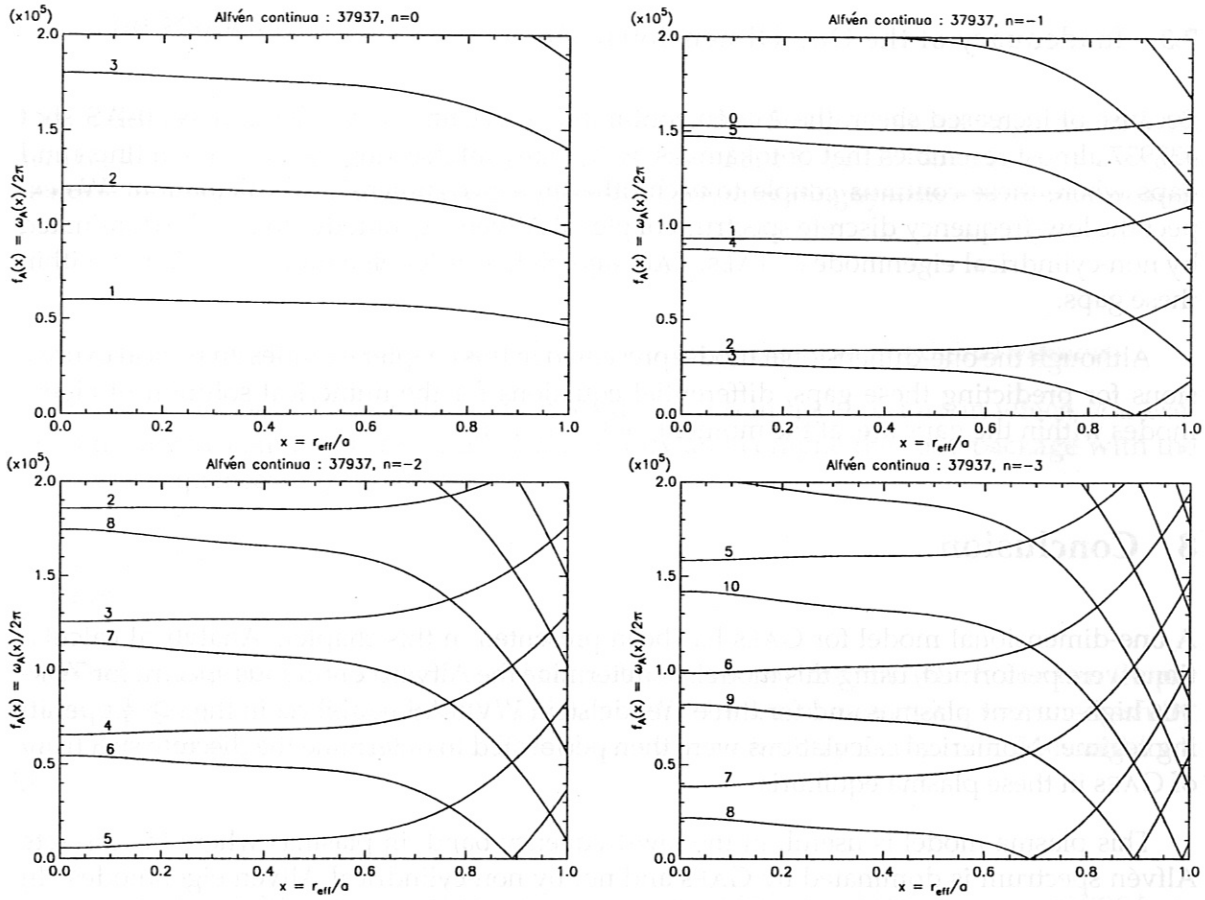

Figure 19: Alfvén continua for Wendelstein WVII-AS #37937. These curves have been calculated in cylindrical geometry and the curves for the $(m, -n)$ mode and the $(-m, n)$ mode are coincident.

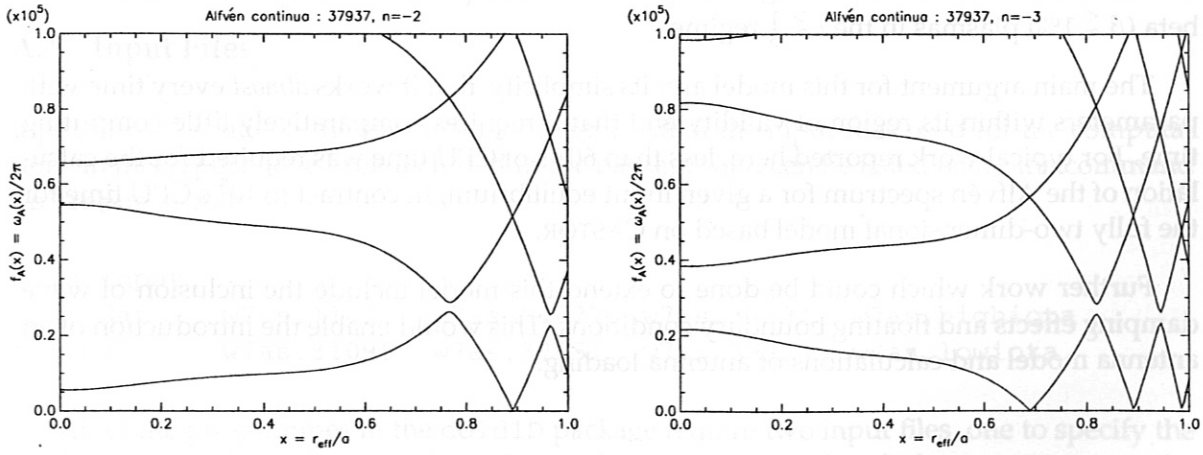

Figure 20: Toroidal coupling in Wendelstein WVII-AS #37937.

7.3 Inadequacy of the One-Dimensional Model

Because of increased shear, the Alfvén continuous spectrum of Wendelstein WVII-AS shot #37937 almost resembles that of tokamaks, with many intersecting cylindrical continua and gaps where these continua couple to each other in a two-dimensional calculation. We expect the low-frequency discrete spectrum of global Alfvén eigenmodes to thus be dominated by non-cylindrical eigenmodes – TAEs, EAEs and higher-order eigenmodes – existing within these gaps.

Although the one-dimensional model presented in this chapter includes analytical expressions for predicting these gaps, differential equations for the numerical solution of eigenmodes within the gaps are, at the moment, not included.

8 Conclusion

A one-dimensional model for GAEs has been presented in this chapter. Analytical calculations were performed, using this model, to determine the Alfvén continuous spectra for TORTUS high-current plasmas and for three Wendelstein WVII-AS equilibria in the $\iota \geq \frac{1}{3}$ operating regime. Numerical calculations were then performed to determine the discrete spectrum of GAEs in these plasma equilibria.

This plasma model is useful, in the low-frequency band, in plasmas where the discrete Alfvén spectrum is dominated by GAEs and not by non-cylindrical Alfvén eigenmodes. In plasmas where non-cylindrical Alfvén eigenmodes dominate the discrete Alfvén spectrum, differential equations based on an asymptotic expansion of the poloidal flux function need to be developed and included into this model so that the eigensolutions corresponding to these wave modes can be determined. In general, this latter scenario corresponds to equilibria where there is significant plasma shear, including most traditional tokamak equilibria. In Wendelstein WVII-AS, low magnetic shear renders the present simple model useful in low-beta ($\beta \lesssim 1\%$) plasmas in the $\iota \gtrsim \frac{1}{3}$ regime.

The main argument for this model are: its simplicity, that it works *almost* every time with parameters within its region of validity and that it requires comparatively little computing time. For typical work reported here, less than 600 s of CPU time was required for the calculation of the Alfvén spectrum for a given input equilibrium, in contrast to 10^5 s CPU time for the fully two-dimensional model based on CASTOR.

Further work which could be done to extend this model include the inclusion of wave damping effects and floating boundary conditions. This would enable the introduction of an antenna model and calculations of antenna loading.

A The Package cold1D

The model described in this paperhas been implemented in the C++ code package cold1D. At the IPP, this code has been archived in /afs/ipp/m/act/distrib/cold1D.tgz and can be extracted on any IBM RISC computer running the AIX operating system with the command:

```
> gtar zxvf /afs/ipp/m/act/distrib/cold1D.tgz
```

Rerun this command anytime you wish to restore all files to their original version.

There should now be a subdirectory named cold1D in the directory in which you executed the above command. Enter this subdirectory and compile the code package with the command sequence:

```
> cd cold1D
> make
```

What should follow is a whole lot of compiler debugging output, which you can (hopefully!) safely ignore. When compilation is complete, check that everything was successfully compiled with the ls -F command. This shows you a directory listing, which should look like:

```
> ls -F
Makefile     ctm*         gae*         include/     lib/         spec*
Makefile.d   ctmtae*      hack/        input/       main/        src/
```

Notice that the four main programmes which comprise the cold1D package, ctm, ctmtae, gae and spec, are present.

A.1 Input Files

Input files all reside in the subdirectory input. All of the input files used for the computations in this report have been included in the package, and can be listed using the command ls input as follows:

```
> ls input
parm.dat     w7as.11474   w7as.34077   w7as.37931   w7as.highiota
tortus       w7as.31096   w7as.37551   w7as.37937   w7as.lowiota
```

All of the programmes in the cold1D package require two input files, one to specify the computation and plot limits and another to describe the vessel and plasma parameters for computation. This package uses standard FORTRAN90-style namelist files for all inputs.

The computation and plot limits are specifyed by default by the file input/parm.dat, although you may use the command-line option -f <Alternative LimitsFile> to specify and alternative limits file (see next subsection). The variables which need to be specified

are straightforward and the file is self-documenting. It can be viewed using the command `cat input/parm.dat` as follows:

```
> cat input/parm.dat
Default limits and plotting variables

&limits
        xmin=0.0, xmax=1.0, fmin=0.0, fmax=0.5,
        mmin=-20, mmax=20, nmin=-5, nmax=5,
/

xmin, xmax = Min and max values of x (normalized radial coordinate)
fmin, fmax = Min and max values of f (frequency, in MHz)
mmin, mmax = Min and max values of m (poloidal mode number)
nmin, nmax = Min and max values of n (toroidal mode number)

&plot
        npts=201,
        cheight=0.8,
        nlbl=3, xlbl = 0.1, 0.4, 0.7,
        dxtext=0.02,
        dytext=0.02,
/

npts = number of points to use in graphs
nlbl = number of text labels to use
xlbl = normalized radial position of the text labels
dxtext, dytext = normalized displacement of text labels from graph
```

You may edit this file with an editor of your choice (eg. `vi`, `emacs` etc.) to change the computational and plot limits. Do not forget to separate all variables with commas (`,`) and also do not forget that text not enclosed by the ampersand (`&`) and the slash (`/`) is ignored by the computer. You may thus place helpful comments in your input files.

The device and plasma parameters are specified in other files. For example, all the calculations in Section 4 of this report were done with the input file `input/tortus`, Section 5 with `input/w7as.11474`, Section 6 with `input/w7as.34077` and Section 7 with `input/w7as.37937`. The file `input/w7as.11474` has comments in it, and can be viewed with the command `cat input/w7as.11474` as follows:

```
> cat input/w7as.11474
W7-AS #11474

&vessel
        R = 2.0, a = 0.179, B = 2.54, Aion = 1, Zion = 1,
/

R = Major radius (in m)
```

```
a = Minor radius (in m)
B = Toroidal magnetic field (in T)
A = Atomic mass number of the ions
Z = Atomic number of the ions

&qprof
        nq = 4,
        aq(0) = 2.78210,
        aq(1) = -0.10383,
        aq(2) = 0.50772,
        aq(3) = -0.26546,
        aq(4) = -0.04175,
/

nq = degree of the polynomial specifying the q-profile

The q profile is given by:
        q(x) = aq(0) + x*aq(1) + x^2*aq(2) + ... + x^nq*aq(nq)
where x is the normalized radial coordinate.

&nprof
        nn = 4,
        an(0) = 9.1729e+19,
        an(1) = -4.0748e+19,
        an(2) = 2.1365e+20,
        an(3) = -6.3496e+20,
        an(4) = 3.7516e+20,
/

nn = degree of the polynomial specifying the density profile

The n profile is given by:
        n(x) = an(0) + x*an(1) + x^2*an(2) + ... + x^nn*an(nn)
where x is the normalized radial coordinate.
```

Use the command `cp input/w7as.11474 input/<name-of-your-choice>` to make copy of this file before editing it.

For WVII-AS, the q-profile can be obtained by inverting the ι-profile given by interpolation from an equilibrium database such as TRANS. The density profile can be obtained from transformed Thomson scattering data.

A.2 Calculating Alfvén Continua

The programme `ctm` calculates the Alfvén continua (equation 17) of a plasma, specified in a form similar to the input file `input/w7as.11474` described in the previous subsection.

The input file must be named on the command line upon execution `ctm`. Optional argu-

ments which can also be given on the command line are the limits file and the plotting device. To run `ctm` with the limits file `input/parm.dat`, with an X-windows terminal and on the input file `input/w7as.11474`, enter:

```
> ctm w7as.11474
```

at the command line, which has an identical effect to entering

```
> ctm -f parm.dat -d XWIN w7as.11474
```

as `input/parm.dat` and `XWIN` are respectively the default limits file and plotting device. If you create your own limits file `mylimits.dat` and wish to produce a colour postscript output file, enter

```
> ctm -f mylimits.dat -d PSC w7as.11474
```

at the command line. This produces a colour postscript plot file `ctm.psc`. If you do not want colour, use the option `-d PS` to produce a black-and-white postscript file `ctm.ps`.

After you have gotten `ctm` running, what follows is a table of limits read from the limits file and a table of parameters read from the input file. You may inspect these tables to ensure that no error occurred in reading from both these files. Several parameters in the limits file are ignored by `ctm`, as they are meaningless in the context of this programme. The ignored variables are: `nmin` and `nmax` from the namelist `&limits` and `dxtext` from the namelist `&plot`.

You will the be prompted for the n number for which you wish to calculate the Alfvén continua. Type in the n number and wait for the programme to finish. Debugging output showing the m numbers and the minimum frequencies of the corresponding Alfvén continua should appear on your screen.

If you use an X-window as your plotting device, you will need to clock the right button of your mouse in the X-window to make it go away when the programme is complete.

To calculate the Alfvén continua with corrections for toroidal coupling (equation 20), use the programme `ctmtae` in place of `ctm`.

A.3 Calculating GAE Eigenfrequencies and Eigenfunctions

The programme `gae` calculates GAE eigenfrequencies and eigenfunctions. The equations (13) are solved for a plasma, specified in a form similar to the input file `input/w7as.11474`.

The command-line options for `gae` are identical to those for `ctm`. The postscript output files for colour and black-and-white are, respectively, `gae.psc` and `gae.ps`.

Data are also read from the limits and input files in an identical manner. The ignored plot variables in `gae` are: `mmin`, `mmax`, `nmin`, `nmax`, `nlbl`, `xlbl`, `dxtext` and `dytext`.

When `gae` is running, you will be prompted to enter the m and n numbers of the GAE whose eigenfunction you wish to find. Enter the two integers, separating them with a space. Debugging output should now appear on your screen.

If you use an X-window as your plotting device, you will need to clock the right button of your mouse in the X-window to make it go away when the programme is complete.

The programme `spec` calculates the spectrum of GAEs present in a particular plasma. It once again takes the same command-line options as the other programmes in the `cold1D` package. It ignores none of the variables in `input/parm.dat`, as all of them are meaningful in its context.

B A Brief Comment on a Two-Dimensional Model

The linear resistive MHD spectral code CASTOR [12], together with the Grad-Shafranov solver HELENA [13], calculates the resistive MHD wave spectra in two-dimensional equilibria. Wave equations are derived from a resistive MHD model for the plasma and solved on meshes representing the calculated equilibria, subject to boundary conditions imposed by perfectly conducting vessel walls, a vacuum region between the walls and the plasma and antennae located in this vacuum region.

Two-dimensional equilibrium models of TORTUS and WVII-AS plasmas are developed using HELENA. Alfvén continuum layers were then identified by using CSCAS [14], a reduced eigenvalue version of CASTOR. A new version of CASTOR [15], modelling the coupling of an external antenna to wave modes in the plasma, was then used to numerically calculate the resistive MHD spectrum of the equilibrium models. This work is described in [16], copies of which are obtainable at the IPP from Dr. A. Weller (L7/205, ext. 1905).

This fully two-dimensional model overcomes many of the shortcomings of the one-dimensional model with two-dimensional "corrections". Where the one dimensional model works quite capably in calculating the Alfvén continuous spectra of tokamak equilibria with relatively simple cross-sectional geometries and of stellarator equilibria with very flat rotational transform ι-profiles, it fails when both geometric complexity and magnetic shear are present in the modelled plasma.

However, there are many limitations in using this two-dimensional model on a three-dimensional stellarator equilibrium. The description of the equilibrium magnetic field in terms of a toroidal field in addition to a poloidal field, generated by a toroidal plasma current, is quite different from the helical field configuration of a stellarator. Furthermore, the changing plasma cross-section of the stellarator plasma needs a fully three-dimensional model for a complete description.

The projection of the stellarator equilibrium field configuration onto a tokamak description worked well. Excellent agreement could be obtained between the stellarator ι-profile and the ι-profile of the two-dimensional model by constructing a simulated toroidal current density J_0-profile in the model, although this procedure is both fiddly and tedious. This points to the need more flexibility in the specification of the magnetic configuration in HELENA. Ideally, we would like to get HELENA to converge to the q-profile of an input equilibrium, instead

of J_0-profile. This would involve re-writing much of the original code.

Fitting a three-dimensional equilibrium into an axisymmetric model poses the problem of choosing a plasma cross-section to use in the two-dimensional equilibrium. The strategy adopted was to use the cross-section of the mid-plane of the antenna, as this enables more realistic representation of the antennae used. A further complication arose, that is that HELENA could not cope with W VII-AS cross-sections which are not top-down symmetric. A definite cause for this problem has not been established, although I suspect that it lies in the simulated J_0-profile required to produce W VII-AS-like ι-profiles in a two-dimensional plasma. The large surface currents required may be causing convergence problems in HELENA.

This problem and the extreme sensitivity of HELENA to the input simulated J_0-profile, even in top-down symmetric geometry, limits the usefulness of modelling W VII-AS plasmas with HELENA and CASTOR.

A study of the dependence of the Alfvén continuous spectrum on the shape of the plasma cross-section was performed. The structure of the Alfvén continuous spectra was found to depend fundamentally on the cylindrical continua, with shaping effects introducing only first-order shifts in frequencies and gap sizes. Poloidal modes couple to each other in non-circular plasma cross-sections, with the strength and nature of this coupling dependent on the shape of the plasma. Although this two-dimensional model may not predict the frequencies to good accuracy, we still expect it to be of limited use in predicting the Alfvén continuous and discrete spectra of a given three-dimensional equilibrium.

References

[1] K Appert and J Vaclavik, *Plasma Phys.* **25** (1982), p 551; R C Cross, *An Introduction to Alfvén Waves*, Adam Hilger, Bristol (1988), p 59.

[2] R C Cross and D Miljak, *Plasma Phys. Control. Fusion* **35** (1993), p 235.

[3] J P Freidberg, *Ideal Magnetohydrodynamics*, Plenum Press, New York (1987), p 44.

[4] M J Ballico and R C Cross, *Phys. Fluids B* **2** (1990), p 467.

[5] S P Hakkarainen, R Betti, J P Freidberg and R Gormley, *Phys. Fluids B* **2** (1990), p 1565.

[6] G Y Fu and J W Van Dam, *Phys. Fluids B* **1** (1989), p 1949.

[7] R Betti and J P Freidberg, *Phys. Fluids B* **3** (1991), p 1865.

[8] W H Press, S A Teukolsky, W T Vetterling, B P Flannery, *Numerical Recipes in C (2nd. ed.)*, Cambridge University Press, Cambridge (1992), p 753.

[9] Annual Report of the Max-Planck-Institut für Plasmaphysik (1988), Garching bei München, p 90.

[10] A Weller, D A Spong, R Jaenicke, A Lazaros, F P Penningsfeld, S Sattler, W VII-AS Team and NBI Group, *Phys. Rev. Lett.* **72** (1994), p 1220.

[11] H Callaghan, J Geiger, C Görner, J V Hofmann, R Jaenicke, P J McCarthy and A Weller, in *Proc. 24th EPS Conf. on Controlled Fusion and Plasma Physics*, Berchtesgaden (1997), *to be published*.

[12] W Kerner, S Poedts, J P Goedbloed, G T A Huysmans, B Keegan and E Schwartz, in *Proc. 18th EPS Conf. on Controlled Fusion and Plasma Physics*, Berlin (1991), Vol 15, Part IV, p 89.

[13] G T A Huysmans, J P Goedbloed and W Kerner, in *Europhysics 2nd Int. Conf. on Computational Physics*, Amsterdam (1990), (ed. A Tenner), World

[14] S Poedts and E Schwartz, *J. Comput. Phys.* **105** (1993), p 165.

[15] G T A Huysmans, W Kerner, D Borba, H A Holties and J P Goedbloed, *Phys. Plasmas* **2** (1995), p 1605.

[16] C-Y Teo, *PhD Thesis*, University of Sydney (1997).